Published in final edited form as:

Nature. 2022 November ; 611(7934): 124–132. doi:10.1038/s41586-022-05328-2.

Behavioural and dopaminergic signatures of resilience

Lindsay Willmore[1], **Courtney Cameron**[1], **John Yang**[1], **Ilana B. Witten**[1,2,✉], **Annegret L. Falkner**[1,✉]

[1]Princeton Neuroscience Institute, Princeton University, Princeton, NJ, USA

[2]Department of Psychology, Princeton University, Princeton, NJ, USA

Abstract

Chronic stress can have lasting adverse consequences in some individuals, yet others are resilient to the same stressor[1,2]. Susceptible and resilient individuals exhibit differences in the intrinsic properties of mesolimbic dopamine (DA) neurons after the stressful experience is over[3–8]. However, the causal links between DA, behaviour during stress and individual differences in resilience are unknown. Here we recorded behaviour in mice simultaneously with DA neuron activity in projections to the nucleus accumbens (NAc) (which signals reward[9–12]) and the tail striatum (TS) (which signals threat[13–16]) during social defeat. Supervised and unsupervised behavioural quantification revealed that during stress, resilient and susceptible mice use different behavioural strategies and have distinct activity patterns in DA terminals in the NAc (but not the TS). Neurally, resilient mice have greater activity near the aggressor, including at the onset of fighting back. Conversely, susceptible mice have greater activity at the offset of attacks and onset of fleeing. We also performed optogenetic stimulation of NAc-projecting DA neurons in open loop (randomly timed) during defeat or timed to specific behaviours using real-time behavioural classification. Both open-loop and fighting-back-timed activation promoted resilience and reorganized behaviour during defeat towards resilience-associated patterns. Together, these data provide a link between DA neural activity, resilience and resilience-associated behaviour during the experience of stress.

Traumatic or stressful life events are often triggers for depression and anxiety. However, out of the general population, only a subset of individuals exhibit these outcomes, whereas others remain resilient[1,2]. Understanding what factors bias individuals towards resilience rather than stress susceptibility is a major scientific goal. Previous work using mice has

✉**Correspondence and requests for materials** should be addressed to Ilana B. Witten or Annegret L. Falkner. iwitten@princeton.edu; afalkner@princeton.edu.

Author contributions L.W., I.B.W. and A.L.F. conceived the project. L.W. and C.C. collected data. L.W. and J.Y. analysed data. A.L.F. and I.B.W. advised on the data analysis. L.W., I.B.W. and A.L.F. wrote the paper.

Competing interests The authors declare no competing interests.

Supplementary information The online version contains supplementary material available at https://doi.org/10.1038/s41586-022-05328-2.

Code availability

All code is available on GitHub (https://github.com/lwillmore/QuantifyingDefeat).

Peer review information *Nature* thanks Anna Beyeler and the other, anonymous, reviewer(s) for their contribution to the peer review of this work.

focused on risk factors for susceptibility and pathology following stress[3–8,17–23]. Less attention has been paid to the experience of stress itself. Alterations to the midbrain DA system, crucial in the regulation of reward-based motivation and learning[9,11,12,24–27], have been observed in animals after stress[3,5,6]. Furthermore, modulation of this system following stress can rescue depressive-like phenotypes[4,23]. However, whether DA has an active role during stress in determining outcomes is unknown. Here to understand the links between the experience of stress, behaviour and DA neural activity, we first take advantage of recent developments in computer vision and posture tracking[28] to precisely quantify the actions of mice as they undergo chronic social defeat stress. We then test whether there are changes in the activity of two DA projections aligned to key behaviours during chronic stress. We identify resilience-specific behavioural and neural activity patterns during stress. We also demonstrate that behaviour-triggered DA terminal stimulation during stress is sufficient to prevent susceptibility.

Behavioural signatures of resilience

To detect individual differences in resilience and susceptibility to stress, we subjected mice to a chronic defeat stress paradigm[29] (Fig 1a). Individuals underwent ten consecutive days of defeat in a series of exposures to new aggressors and then were subjected to post hoc behavioural tests to assess resilience (Extended Data Fig. 1a). In accordance with previous work[3], we observed that following the 10 days of defeat, males exhibited different levels of socially avoidant and anhedonic behaviour, which resulted in a spectrum of susceptibility to resilience. To identify resilient and susceptible individuals following the defeat stress, we used a social interaction (SI) test, in which mice freely explored an arena with a new aggressor behind a mesh barrier (Fig. 1b). Unstressed control mice ($N = 22$ mice) spent 51.6 ± 9.65% (mean ± s.d.) of the time in the chamber near the restrained aggressor (SI time). By contrast, stressed animals ($N = 32$ mice) were less social and more variable in the time spent in the arena (40.9 ± 16.7%, t-test for equal means $t = 2.66$, $P = 0.01$, Levene test for equal variance $W = 5.46$, $P = 0.02$). Stressed mice were defined as 'susceptible' if they had SI times less than one standard deviation below the mean from unstressed controls; otherwise they were considered 'resilient' (Fig. 1b and Extended Data Fig. 1b). The distance travelled during the SI test was not significantly different across control, resilient and susceptible groups ($F_{(51,2)} = 0.29$, $P = 0.75$). Susceptible mice also showed anhedonia-like behaviour in the sucrose preference test[30], consuming significantly less sucrose than resilient mice (Extended Data Fig. 1c,d; one-way analysis of variance (ANOVA) $F_{(51,2)} = 3.21$, $P = 0.048$). Additionally, resilience was associated with more weight gain during the 10 days of defeat stress (Extended Data Fig. 1e,f; generalized estimating equation (GEE) (a linear model that accounts for correlated repeated measurements from each mouse over time), $N = 32$ mice, $Z = 2.01$, $P = 0.045$). Stressed mice showed reduced exploration in a two-chamber arena compared with controls, and exhibited fewer chamber crossings (Extended Data Fig. 1g; one-way ANOVA $F_{(51,2)} = 5.77$, $P = 0.006$) and more immobility[31] (Extended Data Fig. 1h; one-way ANOVA $F_{(51,2)} = 3.16$, $P = 0.05$).

Previous studies have reported that resilience is predicted by behavioural and physiological measurements taken before defeat[17–19,21,32]. However, in our data, the pre-defeat weights,

social rank and time spent freely interacting with conspecifics did not predict susceptibility or resilience of the mice (Extended Data Fig. 1e,i–n).

As social behaviours can be highly variable across individuals, we hypothesized that the specific behaviours that the mice engaged in during defeat may predict resilience. Previously, manual labelling has revealed that susceptible animals adopt submissive postures more quickly or flee more than resilient animals[20,22]. To automate behavioural quantification, we recorded every defeat session using 120 Hz videography with both top and side acquisition (Fig. 1c). Body parts of the interacting mice were tracked using markerless pose-estimation software[28] (Fig. 1d). From these body part locations, we defined 12 features to describe the relative and global postures of the mice (Fig. 1e) to identify the following 4 behaviours of interest: (1) being attacked, (2) being investigated, (3) fighting back and (4) fleeing (Fig. 1f). To automate behaviour identification across our large video dataset (around 14 million frames), we trained binary random forest classifiers to use these features to predict human labelling of each of these behaviours (Fig. 1g,h, performance on held-out videos). Resilient and susceptible mice experienced similar levels of attack, which suggested that resilient animals do not undergo a less stressful experience (Fig. 1i). However, we identified modest behavioural differences in two other classified behaviours. First, susceptibility was associated with more investigation from the aggressor (Fig. 1i; GEE, $N = 32$ mice, $Z = -2.05$, $P = 0.040$). Second, resilience was related to fighting back more often while being attacked (Fig. 1i; GEE, $N = 32$ mice, $Z = 2.42$, $P = 0.016$; see Extended Data Fig. 2 for longitudinal changes in behaviour).

To complement supervised classification and to describe behaviour in a more holistic manner, we used unsupervised clustering to generate behaviour maps. To do this, we embedded the same 12 features from each video frame (Fig. 1e) into a 2D *t*-distributed stochastic neighbour embedding (*t*-SNE) manifold (a nonlinear dimensionality reduction technique to preserve local similarity in data). The embedding process retained structure from the original feature space, such as the distance between animal centroids (Fig. 1j and Extended Data Fig. 3a). We discretized behaviour space into 18 clusters that represented areas of peak occupancy, which, for interpretability, we numbered from those in which mice were closest together (1) to furthest apart (18) (Fig. 1k). Differences in individual cluster occupancies between susceptible and resilient individuals were small. However, individuals could be classified into resilient or susceptible groups above chance accuracy using the set of all 18 cluster occupancies. This result indicated that there were differences in overall behavioural strategy (Fig. 1l–n and Extended Data Fig. 3b; 81.25% accuracy on correct classification in leave-one-mouse-out cross validation; for each mouse, a model was trained on all other mice and tested on the held out mouse). Descriptions of the behaviour in a *t*-SNE cluster could be derived from the distribution of original features in the cluster (Extended Data Fig. 3a), the density of expression of random-forest-detected behaviours in the cluster (Extended Data Fig. 3c) and example video frames from the cluster. The four most informative clusters to differentiate susceptible and resilient groups included a proximal and distant behaviour that was more often expressed by each group (Fig. 1l,m). The most resilience-associated proximal cluster (*t*-SNE 1) overlapped with fighting-back frames as identified by the random forest (Fig. 1o and Extended Data Fig. 3c). The most susceptibility-associated proximal cluster (*t*-SNE 3) (Fig. 1p) was characterized by being

investigated in the head and neural implant, consistent with passive freezing[33] and receiving orofacial sniffing[34,35] (related to social subordination). The most susceptibility-associated distant cluster was cluster (*t*-SNE 16) 'avoidance', facing away from the aggressor (Fig. 1q). The most resilience-associated distant cluster (*t*-SNE 15) was a posture of distant 'vigilance'[36] (Fig. 1r).

Females, like males, can exhibit social avoidance and anxiety-like behaviours consistent with resilience and susceptibility following stress[37–39]. However, much less is known about the drivers of individual variability in females. The behaviours that we identified in males as being resilience-associated may be sex-specific defensive strategies. Therefore, we exposed females to 10 days of defeat and explored whether they also have behaviour patterns associated with resilience. To produce aggression towards females, we virally expressed a Cre-dependent excitatory DREADD in the ventromedial hypothalamus ventrolateral area (VMHvl) of *Esr1*::*cre* aggressor males, and these animals were injected every day with clozapine *N*-oxide (CNO) before defeat[38,40] (Fig. 1s). As in males, we identified resilient and susceptible females on the basis of post hoc SI times relative to an unstressed control group and performed additional post hoc testing (Extended Data Fig. 4a–e). Expression of supervised behaviours (being attacked, being investigated, fighting and fleeing) did not differ between resilient and susceptible females (Extended Data Fig. 4f). Moreover, female animals exhibited significantly less fighting-back behaviour compared to males (Extended Data Fig. 4g; $t = -7.45$, $P = 6.2 \times 10^{-9}$), which indicated that the relationship between this behavioural response strategy and resilience may be specific to males. However, unsupervised analysis of female behaviour during defeat revealed a single behavioural cluster (*t*-SNE 5) that was significantly correlated with resilience (Fig. 1t,u; GEE, $N = 8$ mice, $Z = 4.58$, $P = 4.8 \times 10^{-6}$, Bonferroni-corrected for comparisons across 18 clusters). In this cluster ('close vigilance'), mice were in moderate proximity to and facing the aggressor (Fig. 1v and Extended Data Fig. 3a). Together, these data uncovered a new posture associated with resilience and suggest that attack-response behaviours (fighting compared to fleeing) are not associated with resilience in females.

Dopaminergic signatures of resilience

We next tested whether individual differences in neural dynamics during defeat behaviours would also differentiate resilient and susceptible individuals. Differences in spontaneous activity of dopaminergic neurons recorded after the 10 days of defeat stress have been shown to differ between resilient and susceptible individuals[3,5,6]. However, DA neural activity during defeat stress itself has not been described. In addition, different DA projections in the striatum have different functions[24]. DA projections to the TS originate from the lateral substantia nigra and are active in response to threatening[13–16] or alarming[41] stimuli. Conversely, DA projections from the ventral tegmental area (VTA) to the NAc respond vigorously to rewards such as palatable food[9–12] and non-aggressive social investigation[42,43].

To record from DA projections to those areas, we implanted optical fibres in the NAc and the TS of males and females genetically expressing GCaMP6f in midbrain DA transporter (DAT) neurons[10]. We then used fibre photometry[42] to measure bulk calcium fluorescence as

a proxy for neural activity and DA release (Fig. 2a, $N = 19$ males, 8 females; in Extended Data Fig. 5, simultaneous fast scan cyclic voltammetry and fibre photometry recordings in the NAc[11] and the TS show that DA concentration and fibre photometry measurements are highly related). We confirmed that TS(DAT::GCaMP6f) projections respond vigorously to threatening air puffs (delivered to the nose of mice while head-fixed) (Fig. 2b, $N = 19$ males, 8 females, $t = 5.11$, $P = 5.4 \times 10^{-6}$; see also Extended Data Fig. 6a,b). Moreover, NAc(DAT::GCaMP6f) projections respond to the approach of rewarding food (Fig. 2c; $N = 19$ males, 7 females, $t = 6.59$, $P = 3.8 \times 10^{-7}$; see also Extended Data Fig. 6c,d).

We next explored how these DA projections[25,26,27,44] may differently encode the defeat experience in resilient and susceptible mice. Recordings were performed from both sites on each day of defeat and during post hoc testing.

First, we examined the relationship between DA neural activity in the TS and the NAc and physical distance to the aggressor (Fig. 2d). In both males and females, TS(DAT::GCaMP6f) and NAc(DAT::GCaMP6f) projections exhibited opposite profiles in response to aggressor distances (Fig. 2e–g).

In particular, TS(DAT::GCaMP6f) responses increased at the onset of proximity to the aggressor (10.5 cm between-centroid distance) and decreased at the offset (Fig. 3a and Extended Data Fig. 6e), which is consistent with the threatening[13–16] nature of aggressor interactions. This modulation at proximity onset increased across the days of defeat, which indicated that this threat response depended on experience (Fig. 3b; GEE regression for onset activity: main effect of day, $N = 27$ mice, $Z = 4{,}97$, $P = 6.6 \times 10^{-7}$). The magnitude of TS(DAT::GCaMP6f) modulation at proximity onset and offset were similar between resilient and susceptible mice (Fig. 3b,c). However, in females only, susceptibility was related to a greater decrease in activity at offsets (Extended Data Fig. 6f; GEE regression of offset activity: main effect of resilience category, $Z = 3.03$, $P = 0.003$).

In contrast to the TS, we observed that NAc(DAT::GCaMP6f) responses decreased at proximity onsets and increased at offsets, with the magnitude of offset modulation increasing across days (Fig. 3d; GEE regression for offset activity: main effect of day, $N = 27$ mice, $Z = 3.84$, $P = 1.2 \times 10^{-4}$; see also Extended Data Fig. 6g). This is consistent with aggressor proximity being aversive and the end of proximal encounters providing positive 'relief'[43,45,46]. The magnitudes of decrease at proximity onset and increase at the offset were related to susceptibility, which suggests that susceptible individuals experience more aversion to aggressor encounters and relief when encounters ended (Fig. 3e,f; GEE, $N = 27$ mice, onset $Z = 1.98$, $P = 0.032$; offset $Z = -2.77$, $P = 0.006$; see also Extended Data Fig. 6h).

Individual differences in DAT::GCaMP6f measurements in the NAc, but not the TS, in proximity to an aggressor persisted even after the 10 days of defeat, as measured during the post hoc SI test (Fig. 3g–i and Extended Data Fig. 7a–c). Susceptibility was associated with less NAc(DAT::GCaMP6f) responses after entering the social zone (Fig. 3i; Pearson's correlation; $N = 16$ males, 7 females, $R = 0.51$, $P = 0.01$). Neither NAc(DAT::GCaMP6f) responses nor TS(DAT::GCaMP6f) responses during a control behaviour, proximity to a new

object during the SI test, were predictive of resilience (Extended Data Fig. 7d–g). Previous reports have shown that NAc-projecting DA neurons respond to aversive outcomes with decreased activity[14,46]. Our data suggest that across both males and females, DA projections to the NAc reflect greater aversion to the aggressor in susceptible mice compared with resilient ones.

Individual differences in NAc(DAT::GCaMP6f) responses aligned to the onsets and offsets of encounters with the aggressor; our behavioural analysis (Fig. 1i) also suggested that within and around these encounters, resilient and susceptible males may use different attack-response strategies (for example, fight back or flee). These observations led to the hypothesis that DA neural activity patterns associated with these specific behaviours may also differentiate resilient and susceptible males.

To test this hypothesis, we quantified the dynamics of NAc (DAT::GCaMP6f) responses relative to the onsets and offsets of interpretable behaviours identified using our random forest classifiers (being attacked, being investigated, fighting back, and fleeing; Fig. 1f). As defeat-related behaviours can be close in time (for example, frames classified as being attacked and fleeing can be concurrent), behaviour-triggered activity may be difficult to interpret. To account for the contribution of each behaviour to the neural response, we fit the neural activity of each defeated male with a linear encoding model, in which temporally shifted versions of each behavioural event were used to predict neural activity. This resulted in a kernel for each behavioural event, which describes the contribution of that event while accounting for other events[10] (Fig. 4a,b).

Using this model, resilience was associated with increased NAc (DAT::GCaMP6f) responses at the onset of fighting and decreased activity at the onset of fleeing (Fig. 4c; Pearson's correlation, $N = 19$ mice, $R = 0.49$, $P = 0.035$ and $R = -0.8$, $P = 3.7 \times 10^{-5}$, respectively). This result is consistent with a positive relationship between resilience and fighting-back behaviour in males (Fig. 1i). In further support of this, males with increased fight-related activity more often fought back (Extended Data Fig. 8a; Pearson's correlation, $N = 19$ mice, $R = 0.57$, $P = 0.01$). By contrast, susceptibility was associated with less activity at attack onset and more activity at attack offset (Fig. 4c; Pearson's correlation, $N = 19$ mice, $R = 0.47$, $P = 0.041$ and $R = -0.56$, $P = 0.013$, respectively). This provides further support for the notion that susceptible mice exhibit greater aversion at the start of attacks and greater relief when the attacks end[43,45,46].

Anatomical recording location was not correlated with either kernel weights or resilience in either recording location (Extended Data Fig. 8b–d). In contrast to NAc(DAT::GCaMP6f) kernels, TS (DAT::GCaMP6f) kernels did not differ in resilient compared with susceptible males (Extended Data Fig. 8e).

Dopaminergic manipulations during stress

Overall, our recordings of mice during defeat stress revealed that both the behaviours during defeat and the corresponding patterns of NAc(DAT::GCaMP6f) responses are predictive of individual differences in susceptibility and resilience. However, the causal role of NAc

DA during defeat in generating resilience or susceptibility is unknown, as previous studies have not activated DA neurons during the direct experience of defeat. Furthermore, the causal relationship between action-specific patterns of DA neural activity and resilience and susceptibility is not clear. We note that DAT::NAc activity at the onset of fighting was related to resilience and that activity at the offset of attack was related to susceptibility (Fig. 4c). Therefore, one possibility to explore is whether stimulation during these periods will be sufficient to bias individuals towards resilience or susceptibility, respectively.

To address these questions, we performed open-loop (randomly timed) and closed-loop (behaviour-triggered) optogenetic activation during the 10 days of social defeat. This was followed by unstimulated post hoc tests of resilience, including tests of anxiety and mobility. To target DA circuits, *Dat::cre* males were bilaterally injected with an excitatory opsin, and optical fibres were implanted in the NAc (Fig. 5a; $N = 38$ males). After recovery and before defeat, opsin expression was confirmed behaviourally using a real-time place-preference test (Extended Data Fig. 9a). Control animals were implanted with optical fibres but without opsin ($N = 19$ males). To perform closed-loop stimulation, we developed a system for behaviour-triggered optogenetic activation, using fast, online pose detection. We streamed video frames during defeat directly to a trained pose-estimation network, extracted social postural features as previously described (Fig. 1e) and applied a trained binary random forest classifier for our behaviour of interest (Fig. 5b). Phasic light stimulation was triggered contingent on behaviour detection (Extended Data Fig. 9b–f).

We first performed open-loop stimulation during defeat, untimed to behaviour. Phasic bursts of light delivery were randomly distributed throughout behaviour space (Fig. 5c; burst stimulation for 2.99% of the defeat period on average; see also Extended Data Fig. 9d). Even though stimulation was delivered randomly (without respect to ongoing behaviour), we observed behavioural differences in the activation group relative to control animals (Fig. 5d). The most stimulation-biased behaviour, *t*-SNE behaviour cluster 15 (distant vigilance), was identified as informative in predicting resilience in a previous cohort of mice (Fig. 1r). Occupancy of this cluster predicted SI test times in stimulated mice (Fig. 5e). Moreover, stimulated animals exhibited greater SI times relative to controls (Fig. 5f) and had reduced average distance from the aggressor during the sensory period immediately after each defeat (Fig. 5g). Open-loop stimulation also resulted in decreased anxiety in non-social contexts. That is, stimulated animals exhibited more entries into the open-arm areas in the elevated-plus maze (Fig. 5h) and a greater number of crossings in two-chamber exploration than control mice (Fig. 5i). Thus, open-loop DAT::NAc activation, which was not timed to any specific action, increased appetitive social behaviours and increased general resilience following defeat.

Next, we used closed-loop DAT::NAc activation to reinforce fighting back or escape from attack. These behaviours were selected as resilient-associated and susceptible-associated, respectively, on the basis of increased behavioural expression (fight-back, Fig. 1i) and on increased DA neural modulation (fight-back and escape, with escape defined as the offset of proximity following fleeing from attack; Figs. 3f and 4c).

Fight-back triggered DAT::NAc activation increased fighting-back behaviour between early defeat compared with late defeat (Fig. 5j,l; $N = 16$, $t = 2.7$, $P = 0.03$, day 9–10 compared with day 1–2; see also Extended Data Fig. 9g). Compared with controls, animals receiving fight-back-triggered activation more often occupied the 'close vigilance' cluster (t-SNE 5) behaviour that we observed was correlated with resilience in females (Fig. 5k; $t = 2.11$, $P = 0.044$) and had increased SI time during the sensory period of defeat and in the SI test (Fig. 5m,n). Activation timed to fighting back also resulted in increased exploration (Fig. 5o,p) and mobility (Extended Data Fig. 9j) relative to controls, which suggested that these mice had increased resilience beyond social contexts.

Activation of DAT::NAc timed to a susceptibility-associated behaviour (escape[22]) significantly increased the likelihood of fleeing from attack from early to late defeat (Fig. 5s; $N = 8$, $t = 6.4$, $P = 7.2 \times 10^{-4}$, day 9–10 compared with day 1–2; see also Extended Data Fig. 9h). However, the reinforcement of escape behaviour was not sufficient to increase susceptibility (Fig. 5t–w), which suggests that fleeing and its DA neural correlates are reflections of rather than causal drivers of susceptibility.

We next examined whether decreasing DA neural activity during defeat could lead to susceptibility. To that end, we performed attack-triggered closed-loop inhibition of DA neurons in the VTA during defeat. Halorhodopsin (NpHR) was injected bilaterally in *Dat::cre* animals, and stimulation fibres were implanted over the VTA (Extended Data Fig. 9l). Expression was confirmed using real-time place aversion (Extended Data Fig. 9m). Closed-loop inhibition during defeat led to less time being attacked relative to controls (Extended Data Fig. 9r; $t = -3.76$, $P = 0.0012$) and relative to our observation cohort ($t = -7.3$, $P = 5.2 \times 10^{-9}$), perhaps due to behaviour changes in the attack-inhibited animals (for example, reduced fleeing, $t = -3.92$, $P = 8.5 \times 10^{-4}$; Extended Data Fig. 9s). Attack-triggered inhibition did not lead to susceptibility in our post hoc behaviour tests (Extended Data Fig. 9t–x). Thus, although increasing DA neural activity during defeat can bias towards resilience, decreased activity was not sufficient for susceptibility, which is potentially due to the significant reduction in attacks received.

Finally, we asked whether the pro-resilient stimulation paradigms (open-loop and fight-back-triggered) generated profiles of behaviour during defeat (*t*-SNE maps) that resembled the behavioural profiles of resilient animals in our photometry study. Indeed, both open-loop and fight-back-triggered DAT::NAc stimulation during defeat resulted in behaviour patterns during defeat that were more similar to resilient than susceptible animals (Fig. 5d,k,x). These data strengthen the link between resilience-associated behaviour patterns during defeat and resilience. By contrast, experiments that increased avoidance or susceptibility-associated behaviours during defeat (escape-triggered activation and attack-triggered inhibition, respectively) did not promote susceptibility (Fig. 5q–w and Extended Data Fig. 9l–x). We cannot rule out the possibility that targeting other behaviours would have produced susceptibility. However, the observation that opposite manipulations (DA neural activation compared with inhibition during defeat) do not necessarily produce opposite effects (resilience compared with susceptibility) suggests that there may be different mechanisms that contribute to resilience compared with susceptibility. This is

consistent with previous evidence showing that they have separable molecular and synaptic substrates[3,6,47,48].

Discussion

Here we showed that during defeat stress, resilient individuals have behavioural strategies and behaviour-aligned DA neural activity dynamics that differentiate them from susceptible individuals. In addition, activating DAT::NAc during stress not only timed to a resilience-associated behaviour but also untimed to behaviour can bias individuals towards resilience and promote resilient-like patterns of behaviour.

Our observation that DAT::NAc stimulation during defeat can bias towards resilience aligns with previous work[23] showing that stimulation during a different stressor (tail suspension following chronic mild stress) decreases depression-related behaviour. However, our data and that of others suggests that the context of the stimulation may be important in determining whether or not stimulation is pro-resilient. For example, we demonstrated that DAT::NAc stimulation after escape from attack may be less effective than open-loop or fight-back stimulation at driving resilience. Similarly, previous work[4] has shown that stimulation promoted susceptibility rather than resilience when delivered immediately after defeat during the 'sensory period' when the aggressor was separated by a barrier. In both of these examples, DAT::NAc stimulation occurred after aggressor contact had ended and coincided with periods of high endogenous NAc(DAT::GCaMP6f) responses in susceptible mice. Specifically, the escape-triggered stimulation used here was motivated in part by our observation of more DAT::NAc activity after attack or aggressor contact in susceptible mice (Figs. 3f and 4c). Likewise, during the sensory period after the barrier had been replaced, we observed more NAc(DAT::GCaMP6f) signals in susceptible mice (Extended Data Fig. 10), which is consistent with previous reports of enhanced spontaneous firing of DA neurons following defeat in susceptible mice[3,5].

Taken together, this suggests that DAT::NAc stimulation that could be attributed to the aggressor (or any other stressor) is pro-resilient, whereas DAT::NAc stimulation potentially attributed to avoidance or relief from being away from the stressor is not. This hypothesis is in line with the well-established role of DA in promoting positive associations with salient stimuli in the immediate environment[25,26,49], as well as in encoding relief at the offset of aversive stimuli[43,45,46].

In summary, our work highlights the power of combining complex, ethologically relevant social stress paradigms with tools for behaviour quantification[50], chronic and projection-specific neural recording, and behaviour-specific neural manipulations. Elucidating the links between dopaminergic neural activity and behaviour improves our understanding of the role of neuromodulation in mediating individual differences in pathological outcomes.

Online content

Any methods, additional references, Nature Research reporting summaries, source data, extended data, supplementary information, acknowledgements, peer review information;

details of author contributions and competing interests; and statements of data and code availability are available at https://doi.org/10.1038/s41586-022-05328-2.

Methods

Mice

All animal procedures were approved by the Princeton University Institutional Animal Care and Use Committee and were in accordance with National Institutes of Health standards.

A total of 150 experimental animals were used in this study. For the behaviour and fibre photometry recording studies, we used 10 wild-type C57BL/6J males, 40 *Dat*::*cre* (Jackson Laboratory, strain 006660) crossed with the Ai148 GCaMP6f reporter line (Jackson Laboratory strain, 030328)[51,52] males, 6 *Dat*::*cre* males, and 12 *Dat*::*cre* × Ai148 females. For fast scan cyclic voltammetry, we used three *Dat*::*cre* × Ai148 mice. For optogenetics, we used 70 *Dat*::*cre* males and 9 wild-type males. The above mice were naive to non-littermates.

Male and female conspecifics used as social targets in freely moving assays were sexually naive, C57BL/6J mice between the ages of 8 and 26 weeks. Aggressor animals used to deliver chronic social defeat stress were wild-type Swiss Webster (SW) or *Esr1*::*cre* backcrossed to SW strain breeders or retired breeders between the ages of 8 and 57 weeks. Mice were housed in a 12-h light–dark cycle with experiments taking place exclusively during the dark phase. Food and water were given ad libitum. Ambient temperature was maintained at 21–26 °C and humidity at 30–70%. Before behavioural testing, mice were group-housed with 2–5 mice per cage. All animals were bred within the Princeton University animal facilities or purchased from Taconic Biosciences.

Surgery

At 6–12 weeks of age, animals were anaesthetized (isoflurane at 3–5% for induction and 1–3% for maintenance) and placed in a stereotaxic frame before proceeding with injections and implants specific to recording or manipulation experiments.

For GCaMP6f fibre photometry recordings, *Dat*::*cre* × Ai148 mice were implanted with 400 μM core optical fibres in the TS (anterior–posterior (AP): −1 mm; medial–lateral (ML): ±3.25 mm; dorsal–ventral (DV): −2.5 mm relative to the skull surface at bregma) and the NAc (AP: 1.2 mm, ML: ±1 mm, DV: −4.5 mm relative to the skull surface at bregma). One optical fibre was implanted on each hemisphere, with hemispheres randomly selected (MFC_400/430-0.48_3mm_MF2.5_FLT for the TS, and MFC_400/430-0.48_6mm_MF2.5_FLT for the NAc, both from Doric Lenses). Fibres were fixed to the skull with Metabond (Parkell). Then, titanium headplates[53] were secured to the skull of the animals (Ortho-Jet Crystal mixed with carbon glassy, spherical powder, Sigma-Aldrich). Animals were allowed to recover for a minimum of 7 days.

For optogenetic activation, *Dat*::*cre* animals were injected with 500 nl of viral vector expressing an excitatory opsin (ChR2: AAV5-EF1a-DIO-hChR2(H134R)-EYFP/mScarlet-WPRE-HGHpA or ChRmine: AAV5-EF1a-DIO-ChRmine-EYFP/mScarlet-WPRE-HGHPA; produced by the PNI virus core; injected at titre of 7×10^{13} or 5×10^{13} genome copies

per ml) in the VTA (AP: −3.1 mm, ML: ±0.5 mm, DV: −4.71 mm form the skull surface at bregma). In the same surgery or at least 4 weeks later, animals were bilaterally implanted with 200-μM diameter flat optical fibres or 100-μM diameter tapered optical fibres above or within, respectively, the NAc (AP: 1.2, ML: ±1.9, DV: −3.9 to −4.2 mm from the skull surface at bregma, inserted at a 10° angle; un-rotated coordinates of AP: 1.5, ML: ±1.0, DV: −4.5 to −4.8 mm from the skull surface at bregma). No-opsin control animals of the same age (*Dat*::*cre* or negative genotypes) were injected with a virus for EYFP (AAV5-EF1a-DIO-EYFP-WPRE-hGHpA, Addgene, titre of 2×10^{13} genome copies per ml) or received no injection. These animals then received optical fibre implants as described for the opsin-expressing animals. Expression was achieved for a minimum of 8 weeks before behavioural experiments were performed.

For optogenetic inhibition, *Dat*::*cre* animals were injected with 500 nl of viral vector expressing the inhibitory opsin halorhodopsin (AAV5-EF1a-DIO-eNPHR3.0-EYFP-hGHpA; produced by the PNI virus core; injected at a titre of 4.4×10^{13} genome copies per ml) in the VTA (AP: −3.1 mm, ML: ±0.5 mm, DV: −4.71 mm from the skull surface at bregma). In the same surgery, animals were bilaterally implanted with 200-μm diameter flat optical fibres over the VTA (AP: −3.1 mm, ML: ±1.5 mm, DV: −4.2 mm from the skull surface at bregma, inserted at a 10° angle; un-rotated coordinates of AP: −3.1, ML: ±1.2, DV: −4.8 mm from the skull surface at bregma).

For induction of aggression towards females, *Esr1*::*cre* SW males were injected with a viral vector expressing excitatory DREADDs (Elf1a-DIO-hM3Dd(Gq)-mCherry, Addgene 50460; produced by the PNI virus core; titre of 1×10^{14} genome copies per ml). Bilateral injections of 160 nl were targeted to the VMHvl (AP: −4.65 mm, ML: ±0.7 mm from the anterior sinus and DV: −5.8 mm from the brain surface). Incisions were sutured and animals were allowed to recover and virus to express for a minimum of 3 weeks.

Video and fibre photometry data acquisition

For the tube test, chronic social defeat stress, freely moving object and SI tests, and free food reward assay (described below), fibre photometry and videography (BlackFly S camera, FLIR recorded with SpinView software) recordings took place with analog signals monitored simultaneously through a RZ5P data acquisition board (Tucker Davis Technologies).

Specifically, from the camera, we recorded the analog output signal indicating open exposure (using GPIO). The camera was triggered by the recording software at a rate of 120 frames per second (FPS) for chronic social defeat stress and 40 FPS for all others. The camera was mounted 5 cm above and 68.6 cm in front of the recording platform oriented at 90° towards the side of the preparation. For assays other than the tube test, the camera also captured the top-down view of the preparation with a mirror mounted at a 40° angle above horizontal.

GCaMP6f recordings were made through a Doric Lenses photometry system (4-channel driver LEDD_r, LEDs at 465 (and 405 nm in a subset of animals), fluorescence mini cube FMC5_E1(465-480)_F1(500-540)_E2(555-570)_F2(580-680)_S, and Newport Visible

Femtowatt Photoreceiver Module NPM_2151_FOA_FC). The system was driven by and recorded from using custom code written for a real-time processor (RZ5P, Tucker Davis Technologies) in OpenWorkBench (v.2.28.0). GCaMP was excited by driving a 465 nm light-emitting diode (LED) light (about 400 Hz at an intensity of around 10 μW, filtered between 465 and 480 nm) delivered to the brain through a fibre optic patch cord (MFP_400/430/1100-0.48_2m_FCM-MF2.5), with a separate LED and cable for each recording site (NAc and TS). The emission fluorescence passed from the brain through the same patch cords and was filtered (500–520 nm), amplified, detected and demodulated in real time by the system. Demodulated fluorescence signals were saved at a rate of about 1 kHz. Modulation at the 405 nm wavelength was not used for processing GCaMP signals.

Analog camera shutter signals were captured by the processor for synchronization of video and photometry signals.

Separate recordings were made during each behaviour period as follows: 1–10 min during the tube test; 5 min during chronic social defeat stress before the barrier was raised; 5–7 min during defeat while the barrier was raised and attack occurred; 5 min during defeat while the barrier was returned; 5 min during same strain SIs or object interaction; 3–10 min during free food reward; and 5–15 min during head-fixed air-puff delivery.

Behavioural assays

Animals undergoing fibre photometry recordings were subjected to the following assays in this order: tube test, chronic social defeat stress, two-chamber exploration, SI test, sucrose preference test, freely moving object and same strain SI test, free food reward (novelty suppressed feeding in females), and head-fixed air puff. Animals undergoing optogenetic studies were subject to the following assays in order: real-time place preference or aversion (with at least 1 week delay until the next assay), freely moving object and same strain SI test, chronic social defeat stress, two-chamber exploration, SI test, sucrose preference test, freely moving object and same strain SI test, and elevated plus maze test.

Tube test

We used the tube test[54] to establish social rank within the home cage. Before experiencing chronic social defeat stress, 56 mice from 18 cages of 2–5 mice each were evaluated for their social rank within their home cage using the tube test as previously described[55]. For 3 days, mice were habituated to the recording platform and 30.5-cm-long clear plexiglass tube (2.92 cm inner diameter without a ceiling slit or 3.81 cm inner diameter with an elevated floor and ceiling slit for implant access). To habituate, each mouse made ten passes through the tube each day (five from either end).

To test mice for their social rank, for 7 days following habituation, each pair of mice in each cage were placed into the tube such that they met in the middle; every mouse faced each cagemate once per day. From each pair, the loser was defined as the mouse who stepped with a back paw out of the tube and onto the platform first. The other mouse who remained in the tube was defined as the winner. The average percentage of wins per day on the last 3 days of the tube test was used to determine the dominance score of the mouse.

Chronic social defeat stress

Experimental mice were placed in the shoebox home cages (no. 5 expanded mouse cage 22.2 × 30.8 × 16.2 cm, Thoren Caging Systems) of singly housed male SW aggressors. For recording behaviour, food was removed from the cage and the typical stainless-steel lids were replaced with a custom-cut sheet of clear acrylic with a hole or slit for patch cables to run through. Shoebox cages were placed on a platform with an angled mirror, and video recordings were made as described above.

Behavioural and neural recordings were made for 5 min before the barrier was removed, and the SW mice proceeded to defeat the experimental mouse for 5–7 min, during which time recording continued. Finally, the barrier was replaced for an additional 5 min of recording. Stressed animals remained housed opposite the barrier from the aggressor until the following day. For each of the next 9 days, the stressed mice were rotated to be paired with and experience defeat from a new SW mouse. Following the 10 days of defeat, aggressors were removed and all mice were singly housed in the shoebox cages until the remaining stages of the experiment.

Unstressed control animals were pair-housed with a perforated barrier separating the two mice. They were handled and their cages rotated each day for 10 days.

Social defeat stress in females

Defeat procedures and recordings were conducted as described above, but with the following differences in aggressors and overnight housing conditions. Female stressed animals experienced attack from SW aggressors expressing hM3Dd(Gq) in the VMHvl. At 20–40 min before defeat interactions, aggressors were intraperitoneally injected with CNO dihydrochloride (Hello Bio, HB6149) diluted in sterile saline to provide a 0.1 ml injection at a concentration of about 2 mg kg^{-1}. Following behaviour and neural recordings (5 min with barrier, 5 min direct interaction, 5 min with barrier), stressed females were removed from aggressor home cages and housed together, two per cage, separated by a perforated barrier. Unstressed controls were also housed in barrier-separated pairs. Aggressors and females were housed overnight in separate rooms.

SI test

On the next day, following 10 days of defeat stress (day 11), mice were evaluated for resilience using the social interaction (SI) test. First, stressed mice were placed in a two-chamber arena (56 × 24 cm) with two empty mesh pencil cups in the far left and right corners for 5 min. Then the stressed mouse was removed from the chamber, and a new aggressor male SW mouse was placed beneath one cup while a new object (for example, a helping hand clamp) was placed beneath the other. The stressed mouse was then returned to the recording chamber for an additional 5 min. The location of the animal was tracked using Ethovision (Noldus). In particular, we quantified the time spent within the SI and object-interaction zones (6.5 cm from the enclosure). The time spent in the SI zone was used to delineate resilient and susceptible mice. The cut-off was defined as 1 standard deviation below the mean SI time over the unstressed control group.

Freely moving same strain SI and object interaction

Before and after defeat, video and fibre photometry recordings were taken as mice freely interacted with new C57/BL6 social targets of both sexes as well as a new object (for example, a tape roll or a 50-ml Falcon tube). Recordings took place on the same platform as described above for recording defeat. Female social targets were in oestrus, evaluated by vaginal cytology[56]. Behaviour occurred in the same shoebox cages and from the same recording platform used for defeat. After at least 5 min of habituation to the recording cage, mice were presented with the new mouse or object. Video (40 FPS) and fibre photometry recordings were taken for 5 min, beginning immediately before the introduction of the stimulus.

Free food reward

A piece of a palatable treat (mini yogurt drops, Bio-serve F7577, cut with a razor plate into eighths) was dropped into the home cage of the mouse. Videos were hand-scored with BORIS[57] event logging software for approaching (the single food-directed walking bout preceding sniffing and eating), sniffing (nose near the treat without chewing observed) and consuming the food (chewing observed).

Head-fixed air puff

Mice were head-fixed while resting in a sliding plastic burrow[58]. They habituated to the burrow for at least 3 min until they were able to maintain a motionless, neutral position in the burrow. Air puffs (about 15 psi, 6–10 puffs per animal) were delivered to the right whisker pad at manually delivered intervals with at least 10 s between puffs. Animals were required to be in a motionless, neutral position in the sliding burrow before puffs were delivered.

Sucrose preference test

Preference for 1% sucrose (in water) compared to plain water was assessed with a two-bottle choice assay conducted across 3 days, with bottle locations randomly assigned to the left or right of the home cage. The preference was measured as the ratio of sucrose solution to total liquid (water and sucrose) consumed, measured by the difference in the weight of the bottles before and after the 3 days of free consumption.

Two-chamber exploration

Mice were placed in a two-chamber arena (56 × 24 cm) for 5 min. Animal location and speed were continuously tracked using Ethovision (Noldus). From these tracks, we quantified the number of crossings made between the two chambers (defined by centroid passing over the chamber midline) and the amount of time spent immobile (speed < 1 cm s^{-1}).

Novelty suppressed feeding

Females were food-restricted for 18 h before being placed in the corner of a brightly lit, new chamber (49.5 × 49.5 cm) with a single yogurt treat placed in the centre of the chamber on a plastic platform. Latency to consume was scored as the time between entering the chamber

and biting or licking the treat in the centre. After the first consumption bout, animals were placed back in their home cages with ad libitum food access.

Real-time place preference or aversion

Before optogenetic experiments during defeat and at least 8 weeks following virus injections and at least 2 weeks following fibre implantation, mice were tested for opsin expression by preference for the stimulated half of a two-chamber arena (56 × 24 cm). Green (532 nm, 0.8 mW for ChRmine or 4 mW for NpHR animals) or blue (447 or 460 nm, 7–12 mW for ChR2 animals) lasers were connected to a commutator (Doric Lenses, FRJ_1x2i_FC-2FC_0.22), which led to 200-μm diameter patch cords that were fastened to the implants of the mouse through plastic sleeves surrounded by black electric tape. Lasers were triggered by a BNC cable connected to the output channel of a Pulse Pal (https://open-ephys.org/pulsepal), which was programmed to deliver 5 pulses of 5 ms in duration at 20 Hz every 1 s for excitatory opsin animals and continuous light for inhibitory animals.

First, animals explored the chamber for 5 min without receiving light stimulation. Then during a 15 min test period, animals received light stimulation when they were on the designated half of the chamber (alternating sides with animals run in a random order). Mouse centroids were tracked using Ethovision (Noldus) in real-time. When the centroid of the mouse was detected in the stimulated side of the chamber, the software sent a trigger (through a BNC cable connected to the Pulse Pal input port) to run the stimulation protocol as long as the mouse was in the stimulated side. Stimulation was halted when the animal was on the opposite side of the chamber.

Elevated plus maze

Following defeat, animals from the optogenetic study were placed in the centre of an elevated plus maze (2 enclosed arms and 2 open arms, arms 76-cm long and 6.5-cm wide) facing into the open arm away from the experimenter. The animal was free to explore the maze for 7 min while its centroid location was tracked using Ethovision (Noldus). The number of entries into the open arms of the maze was used as a proxy for lack of anxiety.

Behavioural analysis

Behavioural annotation.—For supervised classification of behaviours in defeat, ground truth was determined by manual annotations of videos scored with BORIS[57]. The following behaviours were annotated: stressed mouse being attacked (rapid forward movement of the aggressor such as a lunge or chase directed at the stressed mouse); stressed mouse being investigated (stationary or slow-moving posture with the noise of the aggressor animal close to or in contact with the stressed mouse); stressed mouse fighting back (facing and actively engaged with the aggressor as opposed to leaning back or simply standing near the aggressor); and stressed mouse fleeing (rapidly running or jumping away from the aggressor). The number of annotated frames included 120,983 being-attacked frames out of 896,178 across 25 videos, 51,170 being-investigated frames out of 591,396 across 17 videos, 21,337 fight-back out of 59,1396 across 17 videos and 77,206 fleeing frames out of 896,178 across 25 videos. Annotations were carried out blind to the resilience or susceptibility of the behaving mice.

Markerless pose tracking.—DeepLabCut software (v.2.0.6) was used for tracking the positions of the stressed and aggressor mice during defeat. The training set included 1,000 frames from 70 videos across 21 mice from 3 separate defeat cohorts (as well as 37 outlier frames). The following points were tracked: TopStressNose; TopStressRightEar; TopStressLeftEar; TopStressFibreBase; TopStressTTI; TopStressTTip; TopAggNose; TopAggRightEar; TopAggLeftEar; TopAggTTI; TopAggTTip; BottomStressNose; BottomStressRightEar; Bottom-StressLeftEar; BottomStressFibreBase; BottomStressRightForePaw; BottomStressLeftForePaw; BottomStressTTI; BottomStressTTip; BottomAggNose; BottomAggRightEar; BottomAggLeftEar; BottomAggTTI; BottomAggTTip; TopDividerRight; TopDividerLft; BottomDividerTopRight; BottomDividerTopLeft.

Where, TTip is tail tip, TTI is tail–torso interface, Stress is stressed mouse, and Agg is aggressor. The training was run for 1.03 million iterations with default parameters (training frames were selected using *k*-means clustering of each video session in the training set, trained on 95% of labelled frames, initialized with ResNet-50, batch size of 4).

Feature definition.—To define the posture of the stressed mouse with respect to his environment and the aggressor, we converted pose data to the following behavioural features:

1. Between centroid distance: Euclidean distance between the midpoint between the tail–body interface and nose of each mouse, defined by the top-down view.
2. Distance between aggressor nose and stressed mouse rear.
3. Distance between aggressor nose and stressed mouse nose.
4. Between centroid velocity: instantaneous (every 10 frames or 0.083 s) change in between centroid distance, median smoothed with a window of 0.175 s.
5. Aggressor speed: instantaneous distance between centroid position every 10 frames, smoothed as above.
6. Stressed mouse speed: same details as above.
7. Orientation of aggressor with respect to stressed mouse.
8. Orientation of stressed mouse with respect to the aggressor.
9. Height of the aggressor: side view nose *y* position.
10. Height of stressed mouse: same as above.
11. Distance of stressed mouse from the closest short wall of the cage: based on top-down view.
12. Distance of the defeat mouse from the closest long wall of the cage.

Feature preprocessing.—Features were truncated to fall within the 1st and 99th percentile of all recorded data for each feature (to remove extreme outliers), smoothed across time with a Gaussian filter of 0.25 s and rescaled from −1 to 1

(sklearn.preprocessing.MixMaxScaler) within each session to account for variability in mouse size and slightly varying camera angle or height. We chose to rescale features so that no single feature dominates owing to higher magnitude while maintaining the original feature distributions and their covariances, properties that would not be maintained if each feature were normalized independently to unit variance, for example.

Supervised behaviour classification.—To identify behaviours across our entire video dataset, we trained supervised random forest classifiers using manually annotated data. Behaviours of interest during defeat included being attacked, being investigated, fighting back, and fleeing. These each were classified by a separate binary random forest classifier (Scikit-learn). The training and testing set consisted of eight videos each. Ground truth was determined by manual annotation (BORIS) for frames in which the behaviour was occurring (see above).

For each classified behaviour, the feature matrix included the 12 features described above for each video frame. The objective matrix was a binary indicator if the behaviour was manually annotated in that frame. The training set was composed of all the frames in which the behaviour was present and a randomly selected equal number of frames in which the behaviour was absent. The classifier was trained with a maximum depth of 2 and 100 estimators.

The probability threshold for detecting behaviours was set to the most permissive possible without exceeding a false positive rate of 3% on the training set. Evaluation was conducted by plotting the receiver operator curve on the held-out testing set. The following false positive and true positive rates of classification were obtained: 1.6% and 68%, respectively, for being attacked; 2.7% and 60%, respectively, for being investigated; 2.3% and 56%, respectively, for fighting back; and 2.6% and 53%, respectively, for fleeing.

Unsupervised behaviour embedding and clustering

To characterize behaviours as stereotyped actions repeated throughout time, we followed previous work[59] in using a low-dimensional embedding of the original features and defining behaviours as high density clusters in that low-dimensional embedding. To achieve dense clusters, we embedded our behaviour features using *t*-SNE, which preserves small pairwise distances and thereby retains clustering of nearby points.

Generating this manifold involved a technique known as importance sampling, which enabled us to create a final embedding that included behaviours that might be rare or nuanced, and therefore under-represented in a uniform sampling over time. Importance sampling includes two rounds of *t*-SNE embedding. First, around 12,000 frames of behaviour were uniformly sampled in time across all videos ($N = 348$) analysed for Fig. 1. Those features were embedded into a two-component *t*-SNE manifold (sklearn.manifold.TSNE with perplexity = 100). The embedded space was binned into a 50 × 50 histogram, smoothed with a 2D gaussian kernel of 2.5 standard deviations and parcelated into 18 clusters with watershed (skimage.morphology. watershed) over the smoothed histogram. As *t*-SNE is non-parametric, a separate model was necessary to learn the mapping from the original 12-dimensional feature space to this 2D *t*-SNE space. A

multilayer perceptron (sklearn.neural_network.MLPRegressor, hidden layer size of 400 × 200 × 50 units) was used for this purpose, allowing data from every video frame to be represented in 2D *t*-SNE space, and thus to fall into 1 of the 18 clusters defined in this space.

To generate the final *t*-SNE embedding, we sampled around 10,000 frames from these 18 clusters, with additional sampling of frames in which aggressive encounters took place. To sample from aggressive behaviour, we characterized the overlap between random forest classified attack frames and the clusters in *t*-SNE space. From the cluster that most overlapped with attack, we sampled five random frames from every defeat session. From the 17 remaining non-attack clusters, we sampled 2 random frames from every defeat session. Thus, from 32 males undergoing defeat for 10 days, we sampled (2 × 17) frames from non-attack clusters and 5 frames from the attack cluster on each day for each mouse for a total of 32 × 10 × (17 × 2 + 5) = 12,480 frames. From these sampled frames, we embedded the 12-dimensional behaviour features into two-component *t*-SNE space. The full set of video frames were then mapped into this final *t*-SNE manifold using another multi-layer perceptron. Then a 2D histogram of that perceptron-mapped 2D data was smoothed with a gaussian kernel of 1.5 standard deviations and divided into 18 clusters again with watershed. Gaussian kernels in both *t*-SNE steps were chosen as the roundest number to yield 10–20 clusters from watershed clustering.

Resilience classification by unsupervised behaviour occupancy.—To test whether the amount of time spent in the 18 *t*-SNE-based defeat behaviour clusters was predictive of resilience or susceptibility in individual mice, we assessed leave-one-mouse-out cross-validated accuracy of making binary resilience or susceptibility predictions using logistic regression classifiers (sklearn.linear_model.LogisticRegression, max_iter = 5000, class_weight='balanced', penalty='none'). For each mouse, a single 1 × 18 vector was generated in which each element represented the average fraction of time (across the 10 defeat days) in which that mouse occupied the corresponding *t*-SNE cluster. To avoid collinearity due to the 18 fractions summing to 1, only the first 17 clusters were used in the logistic regression training matrix. In each cross-validation round, the training matrix included an intercept and a chi-square-regularized set of 4 of the 17 *t*-SNE clusters (the 4 clusters with the highest univariate chi-square statistic separating resilient and susceptible mice in the training set, sklearn.feature_selection.chi2). For each held-out mouse, the training matrix was therefore 5 (features) × 31 (mice). For each mouse, there was a new model for a total of 32 models, each with a different held-out mouse. The accuracy was reported as the percent of accurately classified held-out mice. The final model accuracy was 81.25% compared with 50 ± 8.5% (median and s.d.) accuracy in 'correctly' classifying data with shuffled resilience and susceptibility labels.

Relative similarity of unsupervised behaviour profiles

To calculate behavioural similarity between individuals in our manipulation cohorts (Fig. 5 and Extended Data Fig. 9) and between resilient or susceptible populations in our observational cohorts (Fig. 1), we used behaviour embedded in the 2D *t*-SNE manifold described above. For each individual, a behaviour profile was defined as the average across

the 2D smoothed histograms generated from *t*-SNE embeddings on each day of defeat for that individual.

Three population behaviour profiles were then generated: the resilient (R) population in our observation group; the susceptible (S) population in our observation group; and across all mice in our observation (obs) group. The population-level behaviour profiles were defined as averages across profiles from individuals within those populations. Population profiles and profiles from individual mice in each manipulation cohort were each normalized to sum to 1.

The relative similarity between individual profiles (ind) and R or S profiles was defined using the Kullback–Leibler (KL) divergence between maps as follows:

$$\frac{\mathrm{KL}(\mathrm{ind}|\mathrm{R}) - \mathrm{KL}(\mathrm{ind}|\mathrm{S})}{\mathrm{KL}(\mathrm{ind}|\mathrm{obs})}$$

Note that KL divergence is 0 when comparing equal distributions, and larger values indicate larger divergence. Therefore, as presented in Fig. 5x, negative values mean greater relative similarity to R profiles, and more positive values indicate greater relative similarity to S profiles.

Neural analysis

Processing of calcium data.—Each recording session was separately filtered and *z*-scored before further analysis. Demodulated fluorescence signals were processed as follows: removing the linear trend (scipy.signal.detrend; removes downward linear trend due to fibre bleaching); bandpass filtering (0.1–30 Hz, scipy.signal.filtfilt with an order of 3; removes fluctuations outside the timescale of GCaMP6f dynamics); normalizing by a moving average (window of 10 s; converts the signal from fluorescence to change in fluorescence over a moving baseline, that is, $\Delta F/F$); and *Z*-scoring by the standard deviation of the detrended, filtered, normalized signal (normalizes the dynamic range across individuals to allow for comparison between individuals).

Poor-quality recordings ($n = 47$ out of 259 sessions) were removed from further analysis by detecting the fraction of each session in which activity peaks occurred (*Z*-scored signal above 2) and defining poor-quality recordings as those with activity peaks occurring below 2 standard deviations from the average amount of peak activity across sessions (from included animals). If the majority of recording sessions for an animal were excluded, we excluded the remaining sessions from that animal ($n = 5$ out of 26 mice). Animals excluded from neural recording analysis were still included in the behavioural analyses. Animals with poor targeting identified by registering extracted brains to the Paxinos reference atlas were also excluded ($n = 2$ out of 26 mice; Extended Data Fig. 8b).

Linear encoding model.—To capture the linear contribution of behavioural events to the overall observed neural signal, we fit a linear encoding model for each mouse. The objective is to model the *Z*-scored photometry signal during the 10 days of defeat, during defeat interactions, with one set of parameters per animal. We specifically modelled time periods within bouts of close proximity (from 5 s before stressed and aggressor animal centroids

come within 10.5 cm to 5 s after centroid distance goes above 10.5 cm). A single model was fit across all proximity bouts from an individual stressed mouse.

The feature matrix includes representations of eight behavioural events: the onset and offset of each of the four behaviour events of interest quantified by binary random forest classifiers (being attacked, being investigated, fighting back, and fleeing). To make the contributions of these events temporally flexible, we convolved them with a set of cubic splines[10,60]. We chose splines spanning from 1 s before to 2 s after the behaviour to capture both preparatory and reactive neural responses. Then we set the number of splines to seven on the basis of threefold cross-validation accuracy optimized on a linear encoding model. With 7 splines associated with each of the 8 behaviour events, we obtained a total of 56 splines as regressors.

The encoding model takes the form $y = \beta X + \varepsilon$, where y is the photometry signal for a given mouse, with dimension T, or the number of time points across 10 days. X is the design matrix composed of behaviour events convolved with each cubic spline (plus one column of ones for learning the intercept term), with dimensions $57 \times T$. β is the set of weights, one weight for each cubic spline associated with each behaviour type plus an intercept term; the dimensions of β are 1×57. For every behaviour event, we calculated the associated kernel as the sum of seven associated splines of the behaviour event, each weighted by the learned regression coefficients associated with that spline.

Fast scan cyclic voltammetry.—For Extended Data Fig. 5, we recorded fast scan cyclic voltammetry and fibre photometry bulk calcium imaging in the TS from a total of six sites from three male *Dat*:*cre* × Ai148 mice per a previously published protocol[11]. Mice were injected with urethane (1.5 g kg^{-1} dissolved in saline). Once anaesthetized, mice were placed within a stereotaxic frame. A stimulating electrode was inserted into the medial forebrain bundle (MFB; AP: −2.4 mm, ML: ±1.1 mm, DV: −5 mm from the skull surface at bregma). A carbon-fibre electrode extruding 90–110 μm from a pulled glass capillary was adhered to a 400 μm optical cannula (MFC_400/430-0.48_50mm_MF2.5_FLT from Doric Lenses) and inserted into the brain above the TS (AP: −1 mm, ML: ±3.25 mm, DV: −2 mm from the brain surface). A silver-chloride-coated reference electrode was inserted nonspecifically in the brain away from the stimulation electrode and recording sites and adhered with a stainless-steel skull screw.

To make fibre photometry bulk calcium fluorescence recordings, an optical patch cord was attached to the optic cannula, through which a 488 nm excitation laser (400 Hz, 50% duty cycle) delivered excitation, and emission light was received and collected with a photodetector (New Focus, Femtowatt Photoreceiver model 2151). Fluorescence was collected through a USB-powered data acquisition device (USB-201, Measurement Computing) and visualized and stored with TracerDAQ data acquisition software.

The electrode was cycled above the TS by applying a triangular waveform for 10–20 min at 60 Hz, followed by 5–10 min at 10 Hz. Then the electrode was progressively lowered into the brain while calcium recording took place to identify where the fluorescence levels

markedly increased as the electrode entered the striatum. Final recordings were obtained at depths of −2.1 to −2.9 mm below the brain surface.

After entering the striatum, voltammetric recordings (LabVIEW software, National Instruments) took place simultaneously with fibre photometry. In each trial, a triangular waveform was applied at 60 Hz to the recording electrode every 100 ms, and after 5 s of baseline, the MFB was stimulated with pulses of biphasic stimulation (300 μA, 4 ms), after which 25 s of recording was collected for a total of 30 s per recording. For each recording site, 5 trials for each of 1, 6, 12, 24 and 60 MFB stimulation pulses were delivered. We omitted analysis of the 60 pulse trials, as the calcium fluorescence signal saturated at 24 pulses.

Closed-loop, behaviour-triggered activation during defeat.—To deliver light for optogenetic stimulation during specific behavioural time points, we used pre-trained behaviour quantification tools (described above) for inference on video frames streamed in real time.

Images were acquired using a FLIR BlackFlyS camera connected directly to our behaviour inference computer (Ubuntu 16.04, equipped with a Nvidia GeForce RTX 2080 Ti graphics card). Using publicly available custom code, each video frame was captured by a software trigger (PySpin) and sent as an input to our pre-trained DeepLabCut network for estimating the positions of the interacting mice. The 12 features we defined above were calculated with minor modifications (no smoothing, using adjacent frames for instantaneous speed and velocity features). We trained a separate binary random forest classifier to detect fighting behaviour from the unsmoothed features using the same training set as mentioned above for the offline analysis. After detection of a fighting-back video frame, a serial signal was passed through the USB to an arduino, which translated the signal into a TTL for triggering the laser light delivery protocol. The frame capture, behaviour inference and trigger delivery code was run in an open loop and could achieve a speed of about 13 FPS. A list of time stamps from each frame and its probability of behaviour detection and whether a trigger was delivered were saved for synchronization.

To estimate the latency between behaviour detection and light delivery, we measured the differences between the time stamp first real-time video frame of a detected fight-back bout and the next recorded video frame in which a LED that mirrored laser light was illuminated. This latency estimate may be up to 8 ms (1/120 FPS) slower than the true latency because the LED (and therefore laser) may have been illuminated between recorded video camera frames.

Green (532 nm, 0.8 mW for ChRmine animals or 4 mW for NpHR animals) or blue (447 or 460 nm, 7–12 mW for ChR2 animals) lasers were connected to a commutator (Doric Lenses, FRJ_1x2i_FC-2FC_0.22), which led to 200-μM diameter patch cords that were fastened to the implants of mice through plastic sleeves surrounded by black electric tape. Phasic stimulation was delivered through 3 or 5 pulses of 5 ms in duration.

For fight-back-triggered activation, pulses were continuous so long as fight-back behaviour was ongoing to ChRmine animals (compared with being delivered in sets of 5 with a 0.5 s pause between sets for ChR2 animals). In all cases, pulses were 5 ms each at 20 Hz. Laser stimulation pulses were recorded for synchronization.

Open-loop activation animals were defeated concurrently with fight-back-triggered animals and received the same light stimulation but tethered to the behaviour of the neighbour instead of their own.

Escape-triggered activation animals expressed ChRmine and received a set of 3 green light (0.8 mw) pulses at 20 Hz after exiting close proximity to the aggressor (10.5 cm) following attack bouts, in which fleeing was also detected in at least 50% of attack frames.

Attack-triggered inhibition animals expressed NpHR and received 2 s of continuous green light (4 mW) following the onset of an attack.

A separate FLIR BlackFlyS camera was used to record behaviour. The output signals from both the real-time inference camera and the recording camera were saved for synchronization.

Across all stimulation paradigms, stimulation was performed across all 10 days of defeat, but not during post hoc testing.

Whole-brain histology for photometry fibre recovery.—Following the completion of our photometry and behavioural studies, animals were deeply anaesthetized with an injected ketamine and xylazine cocktail, and perfused with 4% paraformaldehyde (PFA) dissolved in 1× PBS. Brains were extracted, post-fixed in 4% PFA for 12–24 h, after which they were cleared using a previously described iDISCO+ protocol[61]. Cleared brains were then imaged with light sheet microscopy at ×1.1 or ×1.3 magnification, and these images were registered to a common reference atlas as previously described[62]. We chose to register to the Paxinos Atlas[63] to access anatomically defined boundaries between the NAc core and shell as well as definitions of subregions in the TS. Fibre tip locations were manually identified in registered light sheet images and plotted together in the common Paxinos coordinate frame.

Histology for optogenetic virus expression and fibre recovery.—Following the completion of our optogenetic studies, animals were deeply anaesthetized with an injected ketamine and xylazine cocktail, and perfused with 4% PFA dissolved in 1× PBS. Brains were extracted, post-fixed in 4% PFA for 12–24 h, after which they were cryoprotected in 30% sucrose and embedded in optimal cutting temperature mounting medium (Fisher Healthcare Tissue-Plus OCT compound, Fisher Scientific) for freezing over dry ice. Cryosections of the frozen tissue (30 μm slices) were made and stamped directly onto glass microscope slides. Slices were washed with PBS or, for immunohistochemistry, PBS+0.4% Triton (PBST). Then, for immunostaining, blocking buffer (PBST with 2% normal donkey serum and 1% BSA) was applied for 30 min, followed by incubation by a primary antibody at 4 °C for 12–24 h. Following primary antibody incubation, slides were washed with PBST (3 rounds of 10 min each) followed by incubation at room temperature in a secondary

antibody for 1 h, and a final set of washes in PBS (3 rounds of 10 min each). Stained or unstained slides were then dried, coverslipped with mounting medium (EMS Immuno Mount DAPI and DABSCO, Electron Microscopy Sciences, 17989-98, lot 180418) and sealed with clear nail polish around the slide edges. After at least 12 h of drying, slides were imaged with a digital robotic slide scanner (NanoZoomer S60, C13210-01, Hamamatsu). The following antibodies were used: anti-GFP molecular probes G10362 (1:1,000 dilution) and rabbit monoclonal; Alexa Fluor 488 Jackson Immuno research 711-545-152 (1:1,000 dilution).

Statistical analysis

Sample sizes were not predetermined ahead of time. Experimenters were not blind to the experimental group assignments of the animals. The following statistical tests were run in Python (v.3.6.12): scipy (v.1.5.2) and statsmodels (v.0.12.0).

Tests for linear relationships were Pearson's correlation (corr, scipy. stats.pearsonr), in which repeated measures were not made, and GEE (statsmodels.formula.api.GEE, groups='mice', family='Gaussian', cov_structure='Independence'), in which repeated measures were made. GEEs are extensions to generalized linear models for longitudinal data, for which no assumptions are made about the normality of the data and inferences are drawn over the population of mice while also accounting for correlations in measurements within each mouse. One-way ANOVA tests (statsmodels.stats.anova.anova_lm) were used when assessing the difference in means across more than two groups, with post hoc *t*-tests (scipy.stats.ttest_ind, equal_var=True, nan_policy='propagate', permutations=None, random_state=None, alternative='two-sided', trim=0) applied when a significant between-group difference was detected. For tests of an interaction between time and more than two groups, a two-way ANOVA (statsmodels.stats.anova.anova_lm, Type=2) was used. For tests with more than two groups, a mixed linear model (statsmodels.formula.api.mixedlm, fixed effects of endogenous variables of interest, and random effects of intercepts for each mouse) was used. To test equality of variance, Levene's test (scipy.stats.levene, centre = 'median') was used. See Supplementary Tables 1–29 for detailed statistical values, model equations and coding of variables. Statistical significance in figures and text is set at $*P < 0.05$, $**P < 0.01$ and $***P < 0.001$.

Reporting summary

Further information on research design is available in the Nature Research Reporting Summary linked to this article.

Extended Data

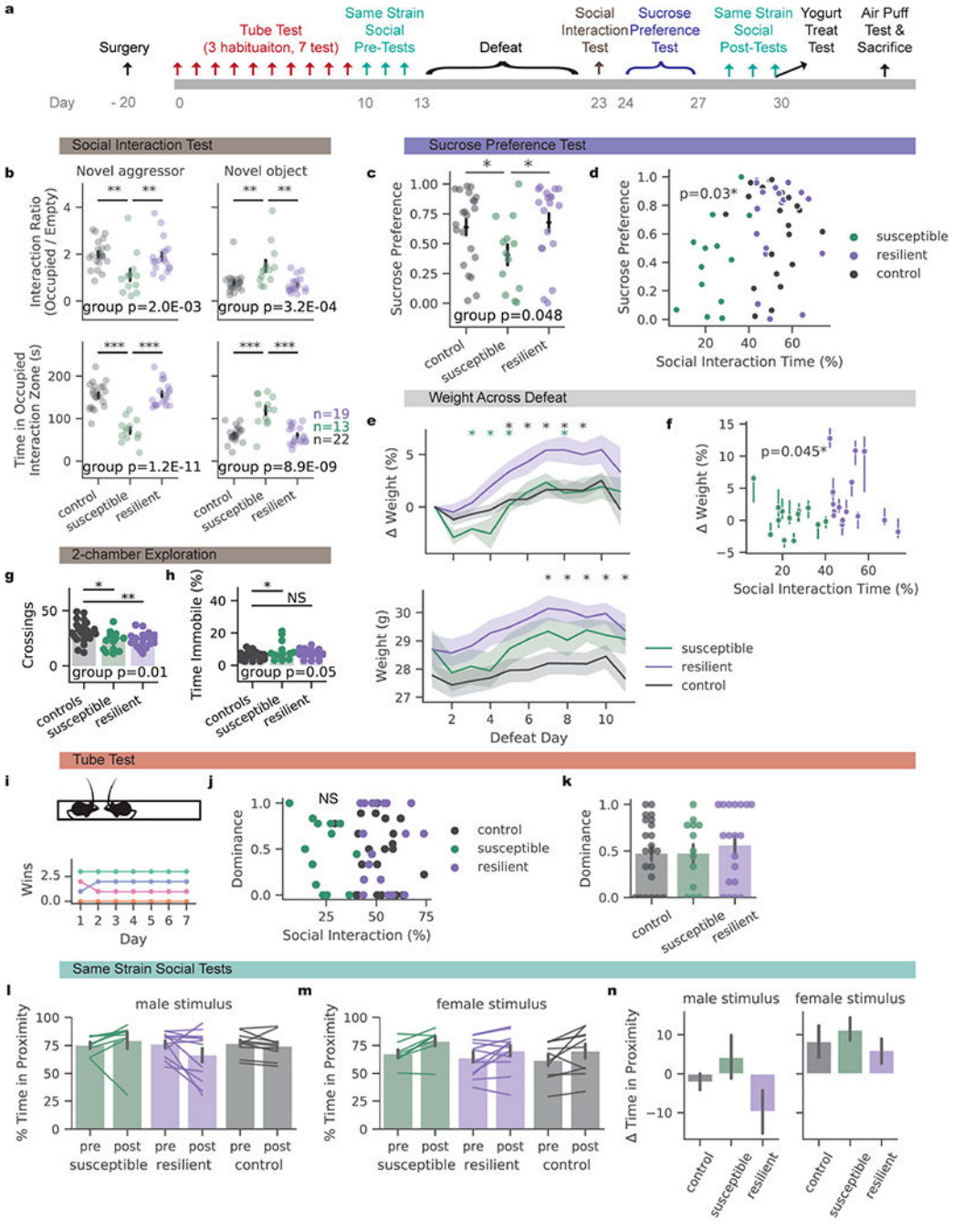

Extended Data Fig. 1 |. Pretests do not predict susceptibility while additional post-hoc tests confirm resilient and susceptible phenotypes.

a, Timeline of behaviors for mice undergoing behavioral and neural recordings across chronic social defeat stress. **b**, In the social interaction test, social interaction ratio and time (N = 22 controls, 13 susceptible, 19 resilient males in **b**–**k**; 1-way ANOVA for social interaction ratio with mouse category as factors, $F_{(51,2)} = 7.015$, p = 0.002, t-Test control vs susceptible p = 0.001, resilient vs susceptible p = 0.009, control vs resilient p = 0.646;

1-way ANOVA for social interaction social interaction time with mouse category as factors, $F_{(51,2)}$ = 42.9, p = 1.18E-11, t-Test control vs susceptible p = 1.6E-9, resilient vs susceptible p = 1.6E-9, control vs resilient p = 0.9). In social interaction test, object interaction ratio and time (1-way ANOVA object interaction ratio with mouse category as factors, $F_{(51,2)}$ = 9.442, p = 3.3E-4; t-Test control vs susceptible p = 0.003, resilient vs susceptible p = 0.001, control vs resilient p = 0.5; 1-way ANOVA for object interaction time with mouse category as factors, $F_{(51,2)}$ = 27.26, p = 8.86E-9; t-test control vs susceptible p = 0.003, resilient vs susceptible p = 0.001, control vs resilient p = 0.6). **c**, Fraction of sucrose over total volume consumed in a 2-bottle sucrose preference test (1-way ANOVA for sucrose preference with mouse category as factors, $F_{(51,2)}$ = 3.21, p = 0.048; t-Test control vs susceptible p = 0.039, resilient vs susceptible p = 0.024, control vs resilient p = 0.9). **d**, Relationship between sucrose preference and SI time (2-sided pearson correlation coefficient R = 0.29, p = 0.03). **e**, Change in weight across defeat (top), absolute weight (bottom), mean±SEM plotted (t-test for difference of means between resilient vs. susceptible and resilient vs. control groups, green stars indicate resilient vs susceptible and black indicate resilient vs control significance, see Supplementary Table 1 for statistical values). **f**, Relationship between SI time and the change in weight during defeat (2-sided GEE, grouped by mouse, Z = 2.01, p = 0.045). **g**, Number of crossings between chambers of a 2-chamber arena (1-way ANOVA for crossings with stimulation groups as factors, $F_{(51,2)}$ = 5.77 p = 0.006; post-hoc t-Test susceptible vs control p = 0.011 and resilient vs control p = 0.008). **h**, Percent of time immobile (speed < 1 cm/s) during exploration of a 2-chamber arena (1-way ANOVA for crossings with stimulation groups as factors, $F_{(51,2)}$ = 3.16 p = 0.05; post-hoc t-Test susceptible vs control p = 0.032 and resilient vs control p = 0.071). **i**, Schematic of tube test for social hierarchy (top), example of tube test wins for a homecage of mice (colored by individual) measured across 7 days. **j**, No relationship between dominance (percentage of wins in the last 3 days of the tube test) and social interaction time in the social interaction test (N = 22 controls, 13 susceptible, 19 resilient; 2-sided Pearson's correlation coefficient R = −0.038, p = 0.78). **k**, Summary of **j** (1-way ANOVA for social interaction social interaction time with mouse category as factors, $F_{(51,2)}$ = 0.342, p = 0.712). **l**, Time spent in proximity with a male of the same strain (C57/BL6), in a freely moving environment (2-way mixed ANOVA with resilience group and time point as factors: group x time $F_{(64,2)}$ = 0.319, p = 0.728) **m**, Time spent in proximity with a female of the same strain (C57), in a freely moving environment. (2-way mixed ANOVA with resilience group and time point as factors: group x time $F_{(64,2)}$ = 0.189, p = 0.828) **n**, Difference in time spent with a male or female social target after vs before defeat, mean±SEM plotted. N = 11 control, 8 susceptible, and 16 resilient males in **l**–**n**. Across panels, *p < 0.05, **p < 0.01, ***p < 0.001.

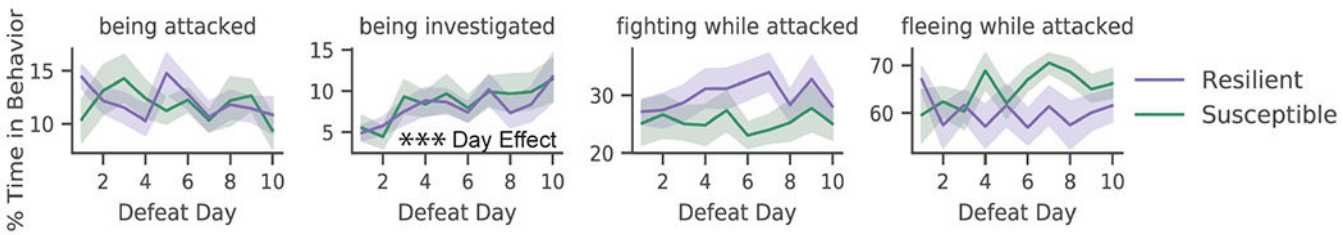

Extended Data Fig. 2 |. Evolution of defeat behaviors across defeat days.

Amount of time spent in classified behaviors across days, mean±SEM plotted (2-sided GEE for time attacked: effect of resilience group Z = 0.23, p = 0.76, effect of day Z = −0.613, p = 0.54; 2-sided GEE for time investigated Z = −0.43, p = 0.66, effect of day Z = 4.01, p = 6.2E-5; 2-sided GEE for fighting while attacked: effect of resilience group Z = 2.09, p = 0.037, effect of day Z = 0.02, p = 0.98, 2-sided GEE for fleeing while attacked: effect of resilience group Z = −1.48, p = 0.14, effect of day t = 1.76, p = 0.078, N = 19 resilient and 13 susceptible mice. *** indicates p < 0.001).

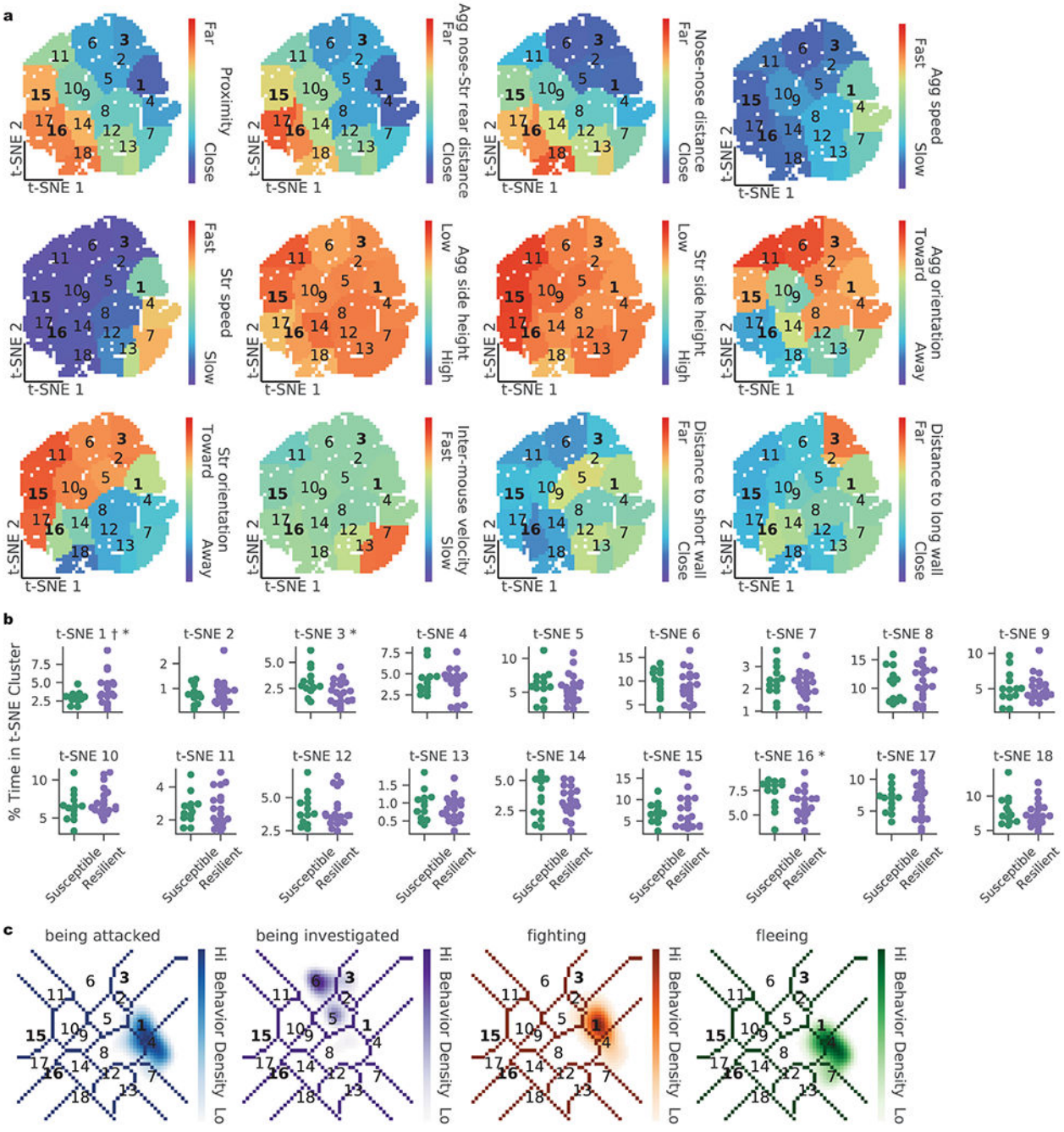

Extended Data Fig. 3 |. t-SNE clusters of social postures represent discrete behaviors, some of which are preferentially occupied by resilient or susceptible mice.

a, Average raw feature value within each t-SNE cluster (scale in the full range of each variable, Str: Stressed mouse, Agg: Aggressor mouse). **b**, Average t-SNE cluster occupancies for each individual, split by susceptible and resilient groups (2-sample, 2-sided T-test *p < 0.05; 2-sample Levene Test †p< 0.05, N = 13 susceptible males and 19 resilient, see Supplementary Table 1 for statistical values). **c**, Density of behaviors annotated with supervised classifiers within t-SNE space, bold font indicating clusters that differentiate resilient and susceptible mice (Fig. 1o–r).

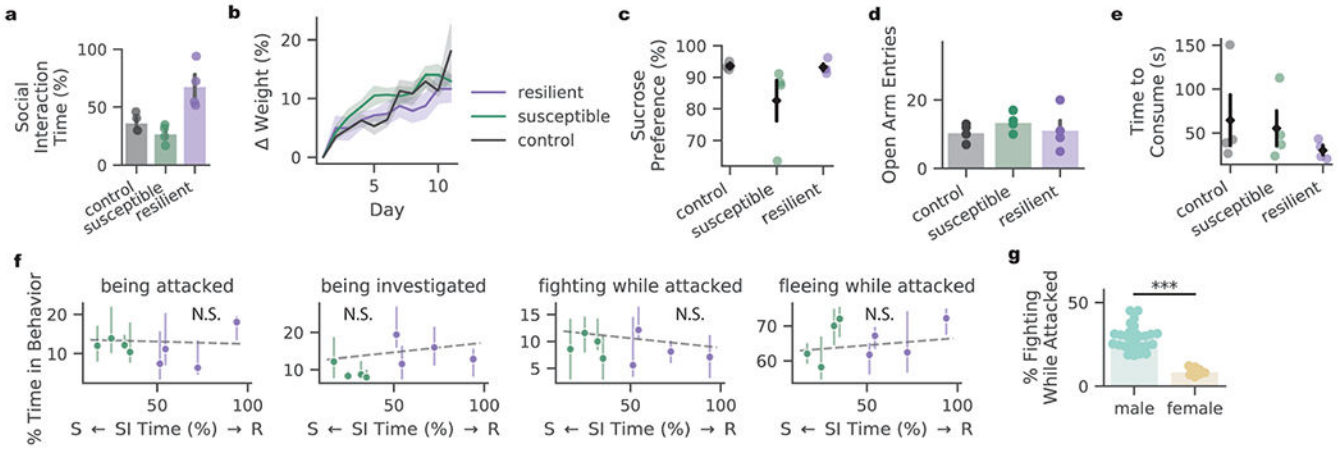

Extended Data Fig. 4 |. Behavioral and physiological differences across defeated females.

a, Distribution of social interaction (SI) times in the post-hoc SI test (see Fig. 1b) in unstressed control and stressed females split into resilient and susceptible groups (N = 4 controls, 4 susceptible, 4 resilient females, mean±SEM plotted). **b**, Change in weight across defeat by females in control, resilient, or susceptible groups, mean±SEM plotted. **c**, Fraction of sucrose over total volume consumed in a 2-bottle sucrose preference test, mean±SEM plotted. **d**, Number of entries into the open arms of an elevated plus maze, mean±SEM plotted. **e**, Time to consume a yogurt treat in novelty suppressed feeding assay, mean±SEM plotted. **f**, Time spent by individual mice in each behavior of interest (2-sided GEE: being attacked p = 0.76; being investigated p = 0.26; fighting while attacked, p = 0.16; fleeing while attacked p = 0.20; means plotted with 30th to 70th percentile error bands across the 10 defeat days; N.S., not significant). **g**, Difference in time males and females spent fighting back while attacked during defeat (2-sample t-Test, t = −7.45, p = 6.2E-9, N = 32 males, 8 females, mean±SEM plotted, ***p < 0.001).

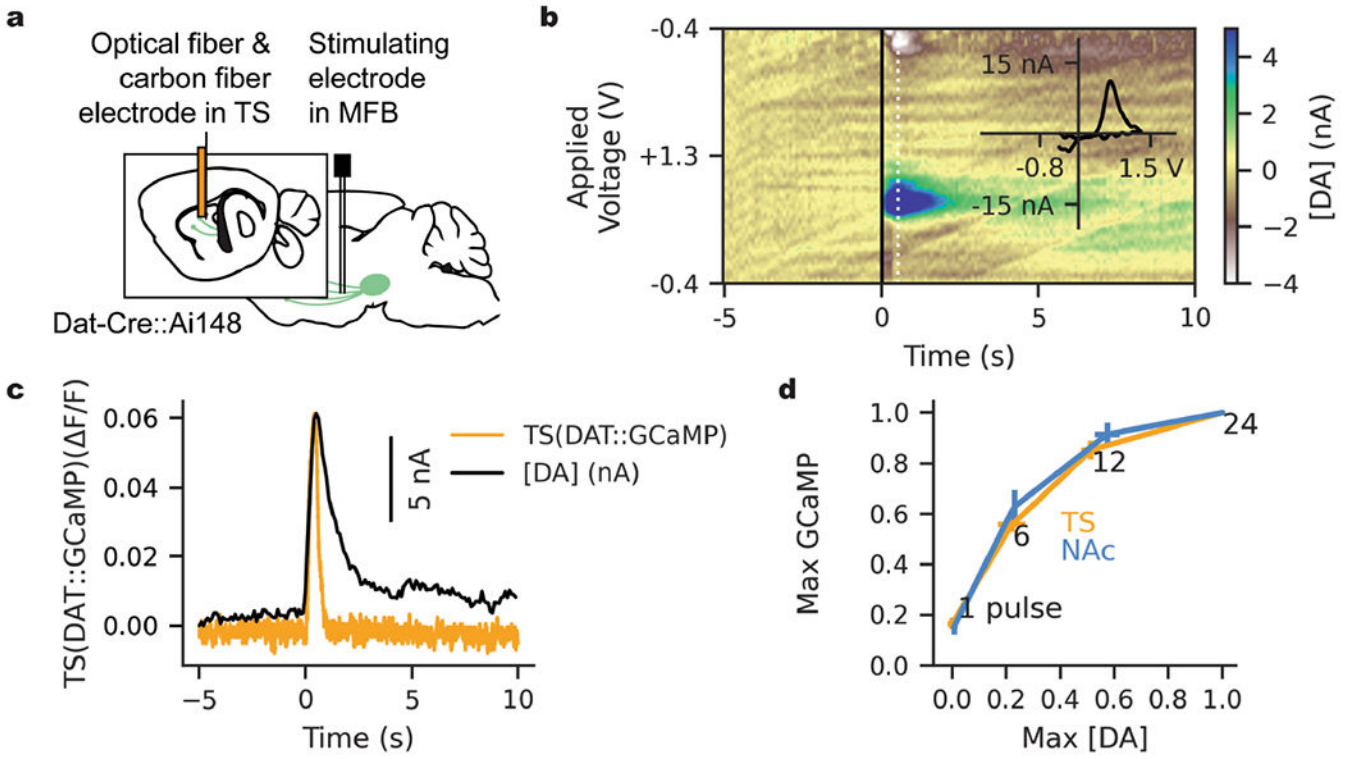

Extended Data Fig. 5 |. Simultaneous fast scan cyclic voltammetry and fiber photometry calcium recordings in the TS.

a, Schematic for recording dopamine release and calcium fluorescence in the tail of the striatum (TS). **b**, Example 3-D color plot from a single recording site, where the medial forebrain bundle (MFB) was stimulated with 24 pulses at 60 Hz at time 0 (average of 5 trials shown). Inset shows the voltammogram at 0.5s after stimulation (white dotted line in color plot), which shows oxidation and reduction peaks consistent with the profile of dopamine. **c**, Time course of simultaneously measured calcium fluorescence and dopamine current (average over the same 5 trials shown in b). **d**, Calcium fluorescence and dopamine concentration peaks increase together with the number of pulses of stimulation delivered to the MFB (mean±SEM plotted, N = 6 recording sites). VTA-NAc data obtained with permission from Parker et al 2016 (N = 4 recording sites).

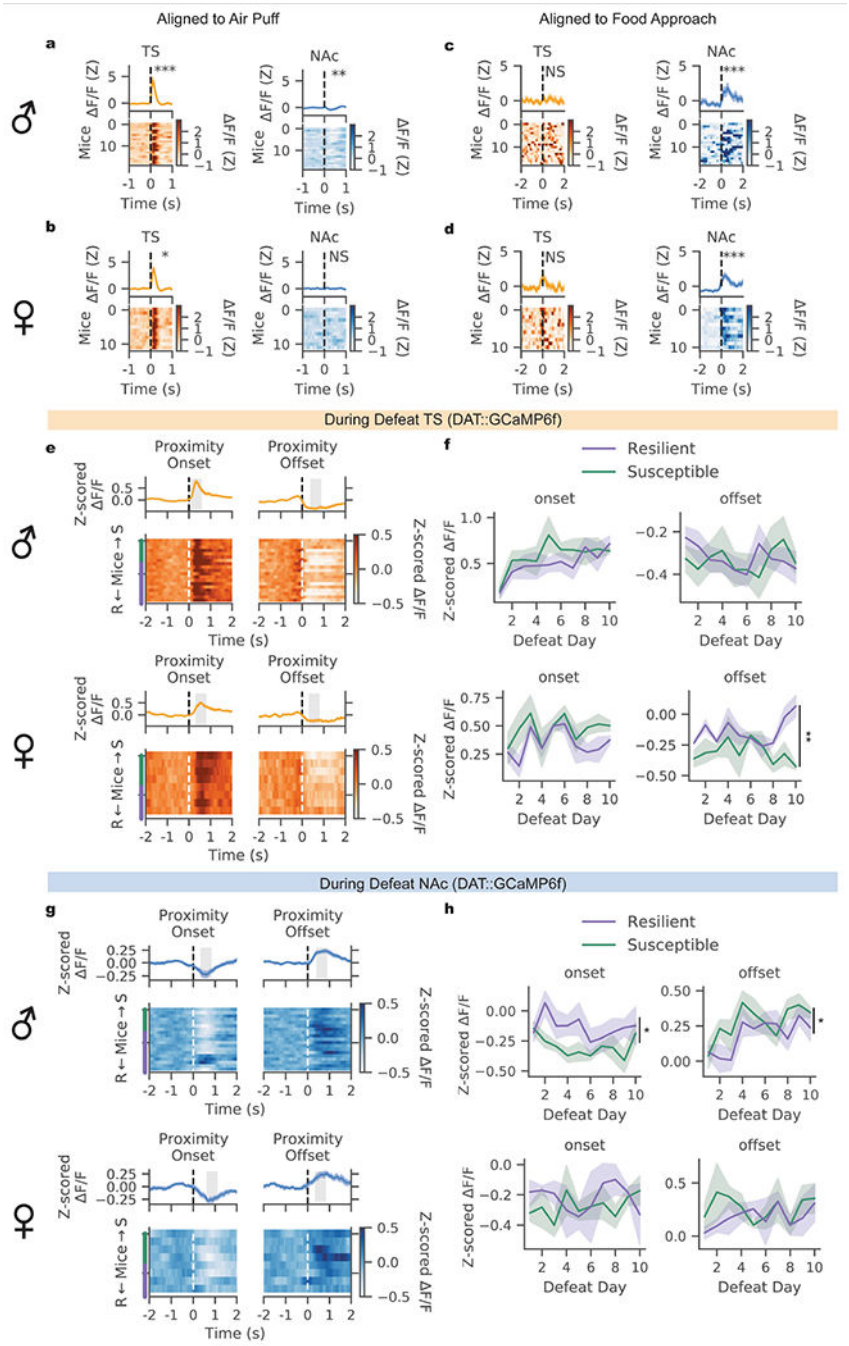

Extended Data Fig. 6 |. DAT::GCaMP6f responses to air puff, food reward, and defeat are similar in males and females.

a, In males, DAT::GCaMP6f aligned to air puff onset, averaged within and across mice (N = 19 males, paired t-Test for average activity after vs before puff, TS: t = 4.61, p = 2.2E-4; NAc: t = −3.1, p = 0.0062). **b**, Same as **a** but in females (N = 12 females, paired t-Test for average activity after vs before puff, TS: t = 3.05, p = 0.011; NAc: t = −1.2, p = 0.25). **c**, In males, DAT::GCaMP6f aligned to palatable food reward approach, averaged within and across mice (N = 18 males, paired t-Test for average activity after vs before approach, TS: t

= 1.63, p = 0.12; NAc: t = 4.31, p = 4.7E-4). **d**, Same as **c** but in females (N = 11 females, paired t-Test for average activity after vs before approach, TS: t = 1.74, p = 0.11; NAc: t = 6.67, p = 5.6E-5). **e**, Average proximity onset- and offset-aligned TS(DAT::GCaMP6f) across stressed males (top) and females (bottom). **f**, TS(DAT::GCaMP6f) in the 0.5s at the onset or offset of social encounters (gray shaded zones in **e**) in males (top) and females (bottom) from resilient and susceptible groups across the 10 days of defeat. Solid line shows mean across mice and shaded region shows standard error. (2-sided GEE regression for male onset activity: main effect of day Z = 5.71, p = 1.1E-8; resilience Z = −0.83, p = 0.407; 2-sided GEE regression for male offset activity: main effect of day Z = 0.45, p = 0.65; resilience Z = 0.107, p = 0.917; 2-sided GEE regression for female onset activity: main effect of day Z = 0.673, p = 0.501; resilience Z = −1.912, p = 0.054; 2-sided GEE regression for female offset activity: main effect of day Z = −1.07, p = 0.28; resilience Z = 3.033, p = 0.003; interaction between day and resilience Z = 2.326, p = 0.02). **g**, Same as **e** for NAc(DAT::GCaMP6f). **h**, Same as **f** for NAc(DAT::GCaMP6f) (2-sided GEE regression for male onset activity: main effect of day Z = −1.328, p = 0.184; resilience Z = 1.98, p = 0.048; 2-sided GEE regression for male offset activity: main effect of day Z = 4.966, p = 6.8E-7; resilience Z = −2.06, p = 0.040; 2-sided GEE regression for female onset activity: main effect of day Z = 1.369, p = 0.171; resilience Z = 1.369, p = 0.402; 2-sided GEE regression for female offset activity: main effect of day Z = −0.074, p = 0.941; resilience Z = −1.29, p = 0.199). Across panels, *p < 0.05, **p < 0.01, ***p < 0.001.

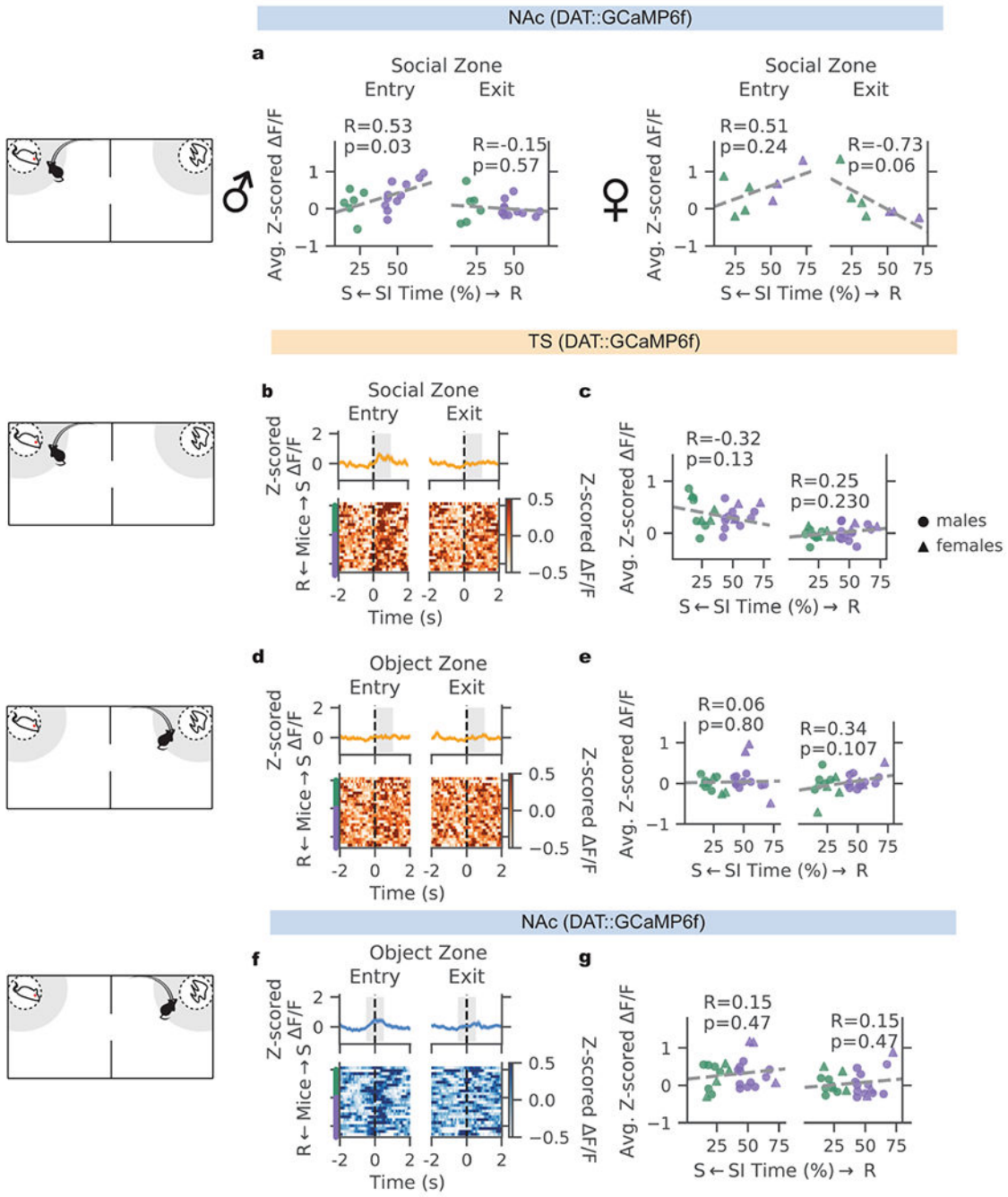

Extended Data Fig. 7 |. In males and females, relationships DAT::GCaMP6f and social zone or object zone entry or exit during the SI test.

a, Same data as in Fig. 2i, separated by male (left, N = 17) and female mice (right, N = 7). (2-sided pearson correlations between GCaMP and social interaction test social interaction (SI) time: Male entry R = 0.53, p = 0.03; male exit R = −0.15, p = 0.57; female entry R = 0.51, p = 0.24; female exit R = −0.73, p = 0.06). **b**, Average social interaction zone entry- and exit-aligned TS(DAT::GCaMP6f) across stressed animals (mean plotted with standard error, N = 6 susceptible males, 4 susceptible females, 10 resilient

males, 3 resilient females in **b**–**g**). **c**, Relationship between individuals' SI time and average TS(DAT::GCaMP6f) in the 1s after entry into the social interaction zone (left, 2-sided pearson correlation, R = −0.32 p = 0.13) and in the 1s after exit from the social interaction zone (right, 2-sided pearson correlation, R = 0.25, p = 0.23). **d**, Average object zone entry- and exit-aligned TS(DAT::GCaMP6f) across stressed animals. **e**, Relationship between individuals' SI test interaction time and average TS(DAT::GCaMP6f) in the 1s after entry into and exit from the object interaction zone (entry: 2-sided earson correlation, R = 0.06 p = 0.8; exit: 2-sided pearson correlation, R = 0.34, p = 0.107). **f**, Same as in **d** for NAc(DAT::GCaMP6f). **g**, Relationship between individuals' SI test interaction time and average NAc(DAT::GCaMP6f) in the 1s surrounding entry into and exit from the object interaction zone (entry: 2-sided pearson correlation, R = 0.15 p = 0.47; exit: 2-sided pearson correlation, R = 0.15, p = 0.47). In **b**,**d**,**f**: mean±SEM plotted.

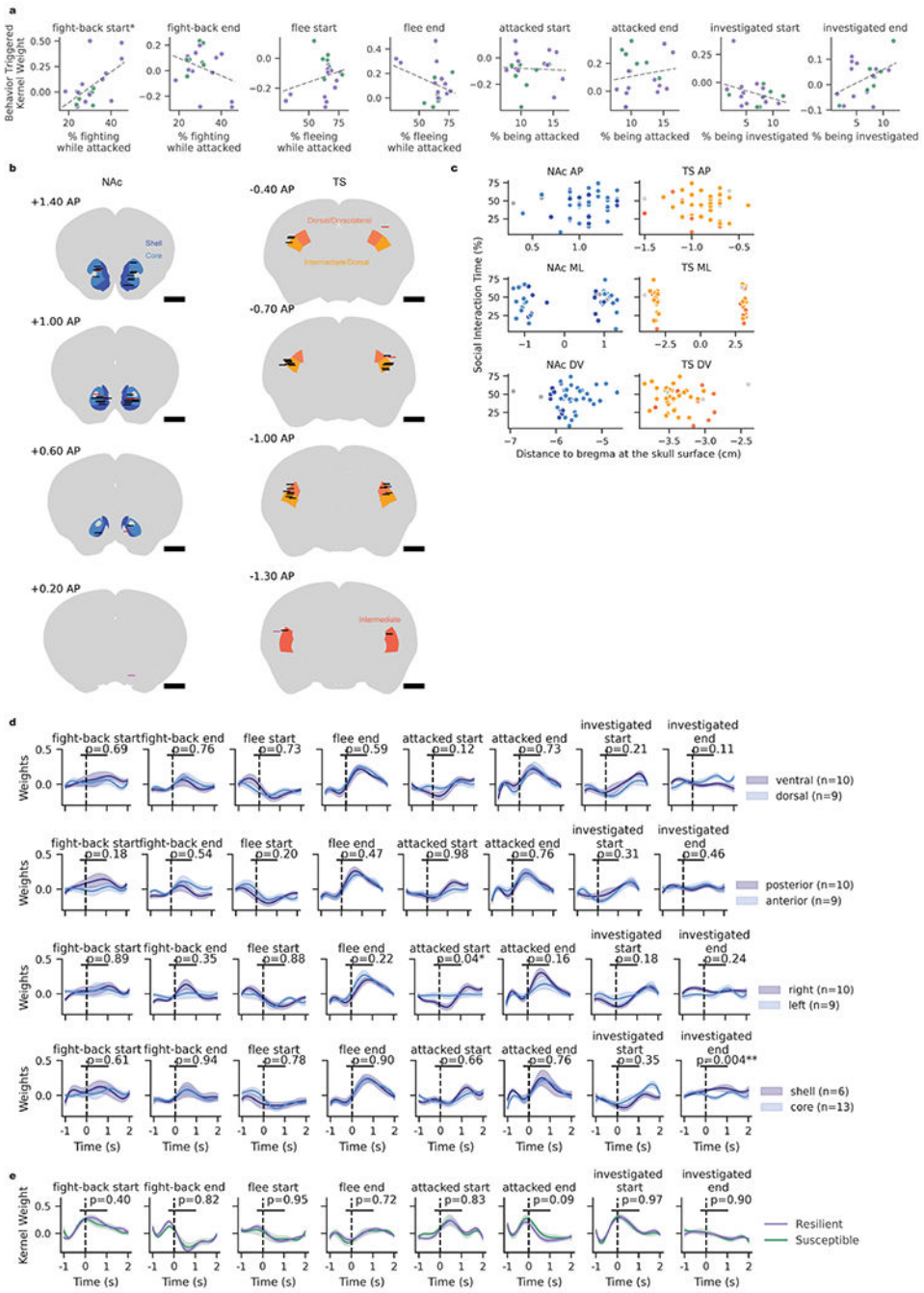

Extended Data Fig. 8 |. Fiber location for photometry recording and behavior encoding by the TS does not predict resilience in males.

a, Relationship between average time spent engaging in each behavior and kernel weight for NAc(DAT::GCaMP6f) encoded by corresponding behavioral events (2-sided pearson correlation, *p < 0.05, N = 19 males, purple designating resilient animals, green showing susceptible, see Supplementary Table 1 for statistical values). **b**, Anatomical locations of photometry fiber tips targeted to the nucleus accumbens (NAc) and tail of the striatum (TS), overlaid on regions defined by the Paxinos Atlas (scale bar 1mm, Paxinos splits

TS into subregions of the caudal caudoputamen). Animals omitted on the basis of poor signal shown in red, or omitted on the basis of poor targeting shown in magenta, included animals shown in black. **c**, Lack of relationship between location of recording fiber tips and SI time. **d**, Average kernel weights for behaviors encoding NAc(DAT::GCaMP6f) in mice grouped by fiber location in the NAc (p-values shown for 2-sided t-test for difference in means in average activity from 0.5 to 1.5s following the behavior event, see Supplementary Table 1 for statistical values). **e**, Average kernel weights for behaviors encoding TS (DAT::GCaMP6f) in mice grouped by susceptibility (p-values shown for 2-sided t-test for difference in means in average activity from 0.5 to 1.5s following the behavior event, N = 7 susceptible (green) and 12 resilient (purple) mice, see Supplementary Table 1 for statistical values). Across panels, *p < 0.05, **p < 0.01.

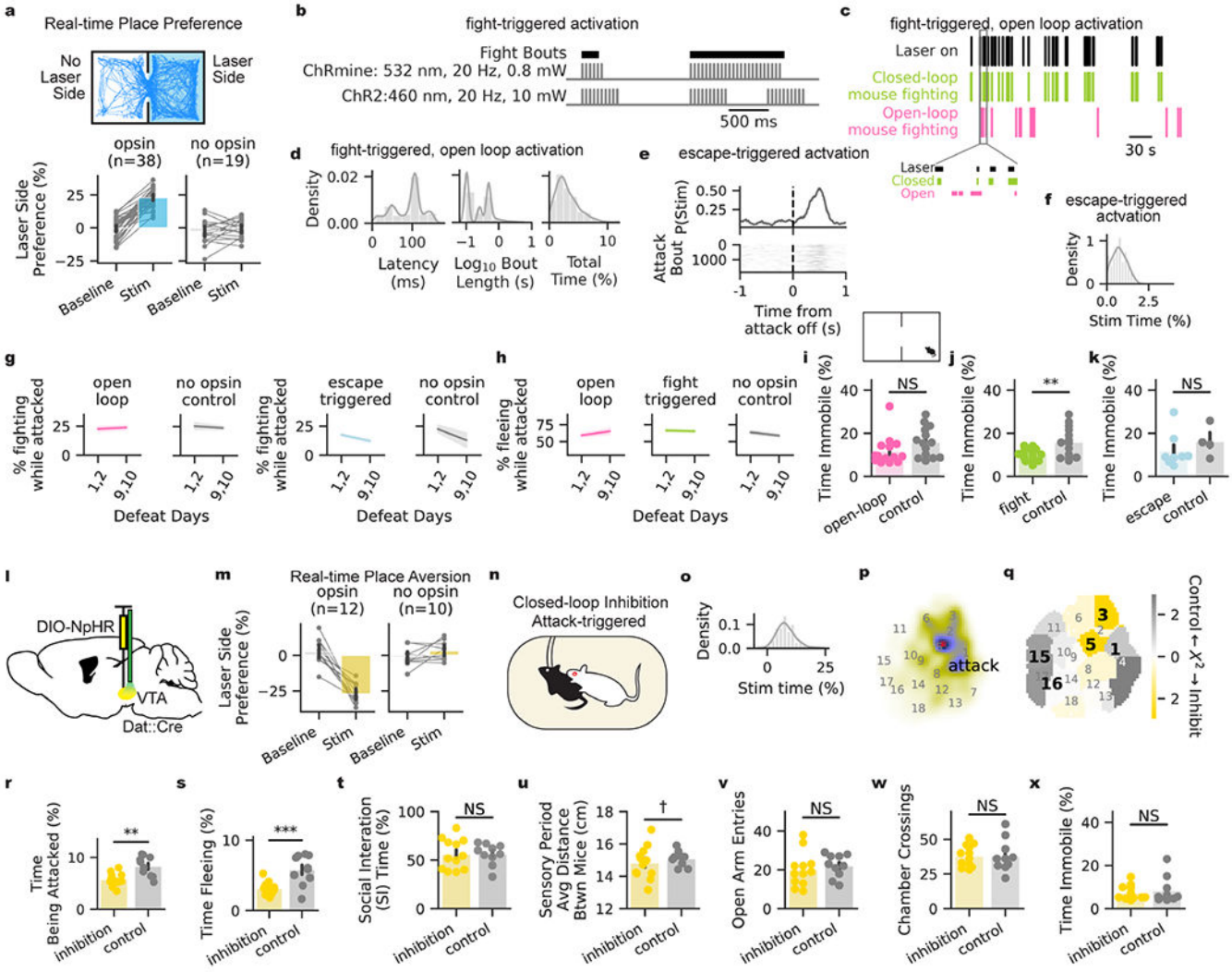

Extended Data Fig. 9 |. Additional characterization of optogenetic manipulation of DA neural activity during defeat.

a, Arena schematic and example stimulation session trace from a 2-chamber real-time place preference assay. 20-Hz laser stimulation was delivered whenever a mouse's centroid was

in the “laser side” of the chamber, sides counterbalanced across mice (top). Preference for the laser-stimulation side of a chamber in mice expressing or not expressing excitatory opsin. No stimulation was delivered in the baseline condition (bottom). **b**, Animals receiving fight-back-triggered optogenetic activation expressed either ChRmine or ChR2 and were delivered 20 Hz laser stimulation with the following parameters: ChRmine mice received green laser stimulation in sets of 3 pulses without pause for the duration of fighting bouts while ChR2 mice received blue laser stimulation in sets of 10 pulses with a 0.5s pause between pulse sets for the duration of fighting bouts. **c**, Example of a defeat session with laser light delivery triggered on fighting of the closed-loop mouse and simultaneously delivered to his open-loop neighbor, bottom inset is a 10s segment. **d**, Statistics across fight-back-triggered stimulation: Distribution of latency to trigger stimulation from capture of a fighting video frame, with a median of 100ms (left). Distribution of durations of stimulation bouts, 94% of which were less than 1s (middle). Distribution of the amount of defeat time in which light was delivered (mean is 2.99% of the defeat session) (right). **e**, Attack-offset aligned laser stimulation during escape-triggered activation. f, In escape-triggered activation, distribution of the amount of defeat time in which light was delivered (mean is 0.75% of the defeat session). **g**, Time spent in random forest labeled fighting behavior early (days 1,2) versus late (days 9,10) in defeat, mean±SEM plotted. (Paired 2-sided t-Tests: 2-way FDR corrected: open-loop t = 0.38 p = 0.71, no opsin t = −0.41 p = 0.71; 2-way FDR corrected: escape-triggered t = −2.33 p = 0.10, no opsin t = −1.14 p = 0.34). **h**, Average expression of random forest labeled fleeing behavior early (days 1,2) versus late (days 9,10) in defeat, mean±SEM plotted. (Paired 2-sided t-Tests: 3-way FDR corrected: open-loop t = 1.12 p = 0.42, fight-triggered t = −0.29 p = 0.78, no opsin t = −1.49 p = 0.42). **i**, Percent of time immobile (speed < 1 cm/s) during exploration of a 2-chamber arena (2-sided t-Test, difference in mean immobility between open-loop (N = 14 males) and no opsin control (N = 14 males) group, mean±SEM plotted: t = −1.57, p = 0.12). **j**, Same as **i** for fight-back-triggered (N = 16 males) and no opsin (N = 14 males) controls, mean±SEM plotted (2-sided t-Test, t = −3.05, p = 0.005). **k**, Same as **i** for escape-triggered (N = 8 males) and control (N = 4 males) groups, mean±SEM plotted (2-sided t-Test, t = −0.80, p = 0.39). **l**, Schematic of inhibition of dopaminergic cell bodies in the VTA (Dio-NpHR injection and fiber implant over the VTA of DAT::Cre males). **m**, Real-time place aversion assay, with constant 7 mW green light delivery on the stimulation side of the chamber. Preference for the non-stimulation side of a chamber in mice expressing or not expressing inhibitory opsin, mean±SEM plotted. No stimulation was delivered in the baseline condition. **n**, Schematic for closed-loop, attack-triggered inhibition during defeat. **o**, In attack-triggered inhibition, distribution of the amount of defeat time in which light was delivered (mean is 7.93% of the defeat session). **p**, Density map of where in t-SNE behavior space animals were when receiving inhibition. **q**, Difference in occupancy of t-SNE clusters between inhibition (N = 12 males) and no opsin control (N = 10 males) groups (same mice in **r**–**x**), measured by individual clusters’ chi^2 statistics; black bold numbers label behaviors differentially expressed by resilient and susceptible mice in our observational study. **r**, Average time across 10 days of defeat being attacked (2-sided -Test, attack-triggered inhibition vs no opsin control, t = −3.03, p = 0.0066). **s**, Average time across 10 days of defeat fleeing (t = −3.92, p = 8.5E-4). **t**, Social interaction (SI) time in the SI test (2-sided t-Test, difference in SI time between inhibition and no opsin control groups: 2-sided t-Test, t = 0.04, p =

0.96). **u**, Average distance between stressed and aggressor mice during the first 5 min of the barrier-separated sensory period across the 10 days of defeat (2-sided Levene test for difference in variance, W = 4.92, p = 0.038). **v**, Number of entries into the open arms of an elevated plus maze (2-sided t-Test, difference in mean entries between inhibition and no opsin control, t = −0.64, p = 0.53). **w**, Number of crossings between chambers of 2-chamber arena (2-sided t-Test, difference in mean crossings between inhibition and no opsin control groups: t = −0.024, p = 0.98). **x**, Percent of time immobile (speed < 1 cm/s) during exploration of a 2-chamber arena (2-sided t-Test, difference in mean immobility between inhibition and no opsin control groups: t = −0.47, p = 0.64). In **r**–**x**, mean±SEM plotted. Across panels, *p < 0.05, **p < 0.01, ***p < 0.001.

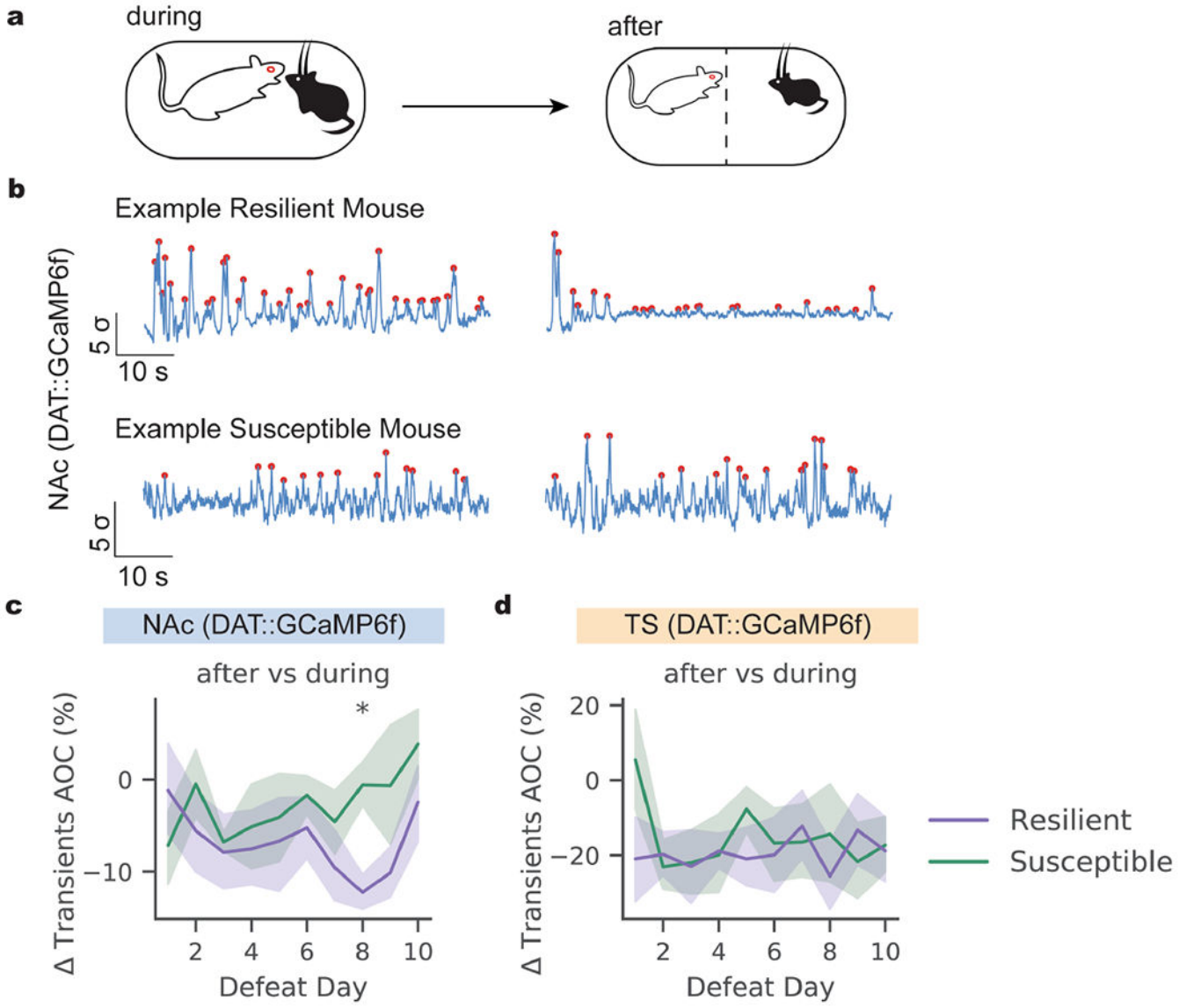

Extended Data Fig. 10 |. Difference in NAc(DAT::GCaMP6f) after versus during direct contact phase of defeat is higher in susceptible compared to resilient individuals.

a, Schematic showing phases of defeat stress during and after direct contact. **b**, Example traces of NAc(DAT::GCaMP6f) during (left) and after (right) the direct contact phase of defeat from day 10 in an example resilient mouse (top) and susceptible mouse (bottom). Transients represented by red dots. Area under the curve (AOC) in next panels refers to the integral between the half max surrounding each transient. **c**, Difference in NAc (DAT::GCaMP6f) after vs during the contact phase of defeat, mean±SEM plotted (Mixed linear model for difference in AOC by day, resilience category, and their interaction; interaction effect N = 19 males, $Z = -2.037$, $p = 0.042$; 2-sided t-Test for difference in ratio of activity in susceptible vs resilient individuals, day 8: $t = -3.607$, $p = 0.02$ after Bonferroni correction for 10 tests across 10 days, $^*p < 0.05$). **d**, Difference in TS(DAT::GCaMP6f) after vs during the direct contact phase of defeat, mean±SEM plotted (Mixed linear model for difference in AOC by day, resilience category, and their interaction; no significant effects).

Supplementary Material

Refer to Web version on PubMed Central for supplementary material.

Acknowledgements

We thank C. Peña, J. Shaevitz and members of the Witten and Falkner laboratories for useful discussions; R. Cho for comments on a previous version of the manuscript; A. Zhukovskaya and A. Minerva for assistance with rebuttal materials; and staff at the PNI Viral Core Facility for reagents and the PNI Brain Registration and Histology Core Facility for assistance with histology. Funding was from NIH T32MH065214 (to L.W.), NSF GRFP DGE-2039656 (to L.W.), NIMH DP2MH126375 (to A.L.F.), NIH R01MH126035 (to A.L.F.), ARO W911NF1710554 (to I.B.W.), NIH R01 DA047869 (to I.B.W.), NYSCF (to A.L.F. and I.B.W.), SCGB (to A.L.F. and I.B.W.), Klingenstein Foundation (to A.L.F.) and an Alfred P. Sloan Fellowship (to A.L.F.). A.L.F. and I.B.W. are New York Stem Cell Foundation Robertson Investigators.

Data availability

The data that support the findings of this study are available on FigShare (https://figshare.com/projects/Behavioral_and_dopaminergic_signatures_of_resilience/141938). Source data are provided with this paper.

References

1. Cohen S, Janicki-Deverts D & Miller GE Psychological stress and disease. J. Am. Med. Assoc 298, 1685–1687 (2007).
2. van Praag HM, de Kloet ER & van Os J in Stress, the Brain and Depression 225–259 (Cambridge Univ. Press, 2004).
3. Krishnan V et al. Molecular adaptations underlying susceptibility and resistance to social defeat in brain reward regions. Cell 131, 391–404 (2007). [PubMed: 17956738]
4. Chaudhury D et al. Rapid regulation of depression-related behaviours by control of midbrain dopamine neurons. Nature 493, 532–536 (2013). [PubMed: 23235832]
5. Cao J-L et al. Mesolimbic dopamine neurons in the brain reward circuit mediate susceptibility to social defeat and antidepressant action. J. Neurosci 30, 16453–16458 (2010). [PubMed: 21147984]
6. Friedman AK et al. Enhancing depression mechanisms in midbrain dopamine neurons achieves homeostatic resilience. Science 344, 313–319 (2014). [PubMed: 24744379]
7. Hultman R et al. Brain-wide electrical spatiotemporal dynamics encode depression vulnerability. Cell 173, 166–180.e14 (2018). [PubMed: 29502969]

8. Peña CJ et al. Early life stress confers lifelong stress susceptibility in mice via ventral tegmental area OTX2. Science 356, 1185–1188 (2017). [PubMed: 28619944]
9. Schultz W, Dayan P & Montague PR A neural substrate of prediction and reward. Science 275, 1593–1599 (1997). [PubMed: 9054347]
10. Engelhard B et al. Specialized coding of sensory, motor and cognitive variables in VTA dopamine neurons. Nature 570, 509–513 (2019). [PubMed: 31142844]
11. Parker NF et al. Reward and choice encoding in terminals of midbrain dopamine neurons depends on striatal target. Nat. Neurosci 19, 845–854 (2016). [PubMed: 27110917]
12. Ikemoto S & Panksepp J The role of nucleus accumbens dopamine in motivated behavior: a unifying interpretation with special reference to reward-seeking. Brain Res. Brain Res. Rev 31, 6–41 (1999). [PubMed: 10611493]
13. Menegas W, Akiti K, Amo R, Uchida N & Watabe-Uchida M Dopamine neurons projecting to the posterior striatum reinforce avoidance of threatening stimuli. Nat. Neurosci 21, 1421–1430 (2018). [PubMed: 30177795]
14. Menegas W, Babayan BM, Uchida N & Watabe-Uchida M Opposite initialization to novel cues in dopamine signaling in ventral and posterior striatum in mice. eLife 6, e21886 (2017). [PubMed: 28054919]
15. Akiti K et al. Striatal dopamine explains novelty-induced behavioral dynamics and individual variability in threat prediction. Neuron 10.1016/j.neuron.2022.08.022 (2022).
16. Tsutsui-Kimura I, Uchida N & Watabe-Uchida M Dynamical management of potential threats regulated by dopamine and direct- and indirect-pathway neurons in the tail of the striatum. Preprint at bioRxiv 10.1101/2022.02.05.479267 (2022).
17. Larrieu T et al. Hierarchical status predicts behavioral vulnerability and nucleus accumbens metabolic profile following chronic social defeat stress. Curr. Biol 27, 2202–2210.e4 (2017). [PubMed: 28712571]
18. Radwan B, Jansen G & Chaudhury D Abnormal sleep signals vulnerability to chronic social defeat stress. Front. Neurosci 14, 610655 (2020). [PubMed: 33510614]
19. Nasca C et al. Multidimensional predictors of susceptibility and resilience to social defeat stress. Biol. Psychiatry 86, 483–491 (2019). [PubMed: 31466563]
20. Wood SK, Walker HE, Valentino RJ & Bhatnagar S Individual differences in reactivity to social stress predict susceptibility and resilience to a depressive phenotype: role of corticotropin-releasing factor. Endocrinology 151, 1795–1805 (2010). [PubMed: 20160137]
21. LeClair KB et al. Individual history of winning and hierarchy landscape influence stress susceptibility in mice. eLife 10, e71401 (2021). [PubMed: 34581271]
22. Murra D et al. Characterizing the behavioral and neuroendocrine features of susceptibility and resilience to social stress. Neurobiol. Stress 17, 100437 (2022). [PubMed: 35242893]
23. Tye KM et al. Dopamine neurons modulate neural encoding and expression of depression-related behaviour. Nature 493, 537–541 (2013). [PubMed: 23235822]
24. Cox J & Witten IB Striatal circuits for reward learning and decision-making. Nat. Rev. Neurosci 20, 482–494 (2019). [PubMed: 31171839]
25. Steinberg EE et al. A causal link between prediction errors, dopamine neurons and learning. Nat. Neurosc. 16, 966–973 (2013).
26. Saunders BT, Richard JM, Margolis EB & Janak PH Dopamine neurons create Pavlovian conditioned stimuli with circuit-defined motivational properties. Nat. Neurosci 21, 1072–1083 (2018). [PubMed: 30038277]
27. Adamantidis AR et al. Optogenetic interrogation of dopaminergic modulation of the multiple phases of reward-seeking behavior. J. Neurosci 31, 10829–10835 (2011). [PubMed: 21795535]
28. Nath T et al. Using DeepLabCut for 3D markerless pose estimation across species and behaviors. Nat. Protoc 14, 2152–2176 (2019). [PubMed: 31227823]
29. Golden SA, Covington HE 3rd, Berton O & Russo SJ A standardized protocol for repeated social defeat stress in mice. Nat. Protoc 6, 1183–1191 (2011). [PubMed: 21799487]
30. Serchov T, van Calker D & Biber K Sucrose preference test to measure anhedonic behaviour in mice. Bio-protocol 6, e1958 (2016).

31. Kudryavtseva NN, Bakshtanovskaya IV & Koryakina LA Social model of depression in mice of C57BL/6J strain. Pharmacol. Biochem. Behav 38, 315–320 (1991). [PubMed: 2057501]
32. Muir J et al. In vivo fiber photometry reveals signature of future stress susceptibility in nucleus accumbens. Neuropsychopharmacology 43, 255–263 (2018). [PubMed: 28589967]
33. Motta SC et al. Dissecting the brain's fear system reveals the hypothalamus is critical for responding in subordinate conspecific intruders. Proc. Natl Acad. Sci. USA 106, 4870–4875 (2009). [PubMed: 19273843]
34. Lee W, Fu J, Bouwman N, Farago P & Curley JP Temporal microstructure of dyadic social behavior during relationship formation in mice. PLoS ONE 14, e0220596 (2019). [PubMed: 31821344]
35. Wesson DW Sniffing behavior communicates social hierarchy. Curr. Biol 23, 575–580 (2013). [PubMed: 23477727]
36. Williams AV et al. Social approach and social vigilance are differentially regulated by oxytocin receptors in the nucleus accumbens. Neuropsychopharmacology 45, 1423–1430 (2020). [PubMed: 32198453]
37. Harris AZ et al. A novel method for chronic social defeat stress in female mice. Neuropsychopharmacology 43, 1276–1283 (2018). [PubMed: 29090682]
38. Takahashi A et al. Establishment of a repeated social defeat stress model in female mice. Sci. Rep 7, 12838 (2017). [PubMed: 28993631]
39. Yohn CN et al. Chronic non-discriminatory social defeat is an effective chronic stress paradigm for both male and female mice. Neuropsychopharmacology 44, 2220–2229 (2019). [PubMed: 31493767]
40. Lee H et al. Scalable control of mounting and attack by $Esr1^{+}$ neurons in the ventromedial hypothalamus. Nature 509, 627–632 (2014). [PubMed: 24739975]
41. Schmack K, Bosc M, Ott T, Sturgill JF & Kepecs A Striatal dopamine mediates hallucination-like perception in mice. Science 372, eabf4740 (2021). [PubMed: 33795430]
42. Gunaydin LA et al. Natural neural projection dynamics underlying social behavior. Cell 157, 1535–1551 (2014). [PubMed: 24949967]
43. Dai B et al. Responses and functions of dopamine in nucleus accumbens core during social behaviors. Cell Rep. 40, 111246 (2022). [PubMed: 36001967]
44. Hamid AA et al. Mesolimbic dopamine signals the value of work. Nat. Neurosci 19, 117–126 (2016). [PubMed: 26595651]
45. Cai LX et al. Distinct signals in medial and lateral VTA dopamine neurons modulate fear extinction at different times. eLife 9, e54936 (2020). [PubMed: 32519951]
46. Wang DV & Tsien JZ Convergent processing of both positive and negative motivational signals by the VTA dopamine neuronal populations. PLoS ONE 6, e17047 (2011). [PubMed: 21347237]
47. Dias C et al. β-catenin mediates stress resilience through Dicer1/microRNA regulation. Nature 516, 51–55 (2014). [PubMed: 25383518]
48. Bagot RC et al. Circuit-wide transcriptional profiling reveals brain region-specific gene networks regulating depression susceptibility. Neuron 90, 969–983 (2016). [PubMed: 27181059]
49. Montague PR, Dayan P & Sejnowski TJ A framework for mesencephalic dopamine systems based on predictive Hebbian learning. J. Neurosci 16, 1936–1947 (1996). [PubMed: 8774460]
50. Datta SR, Anderson DJ, Branson K, Perona P & Leifer A Computational neuroethology: a call to action. Neuron 104, 11–24 (2019). [PubMed: 31600508]
51. Lammel S et al. Diversity of transgenic mouse models for selective targeting of midbrain dopamine neurons. Neuron 85, 429–438 (2015). [PubMed: 25611513]
52. Daigle T L. et al. A suite of transgenic driver and reporter mouse lines with enhanced brain-cell-type targeting and functionality. Cell 174, 465–480.e22 (2018). [PubMed: 30007418]
53. Dombeck DA, Khabbaz AN, Collman F, Adelman TL & Tank DW Imaging large-scale neural activity with cellular resolution in awake, mobile mice. Neuron 56, 43–57 (2007). [PubMed: 17920014]
54. Lindzey G, Winston H & Manosevitz M Social dominance in inbred mouse strains. Nature 191, 475–476 (1961).

55. Fan Z et al. Using the tube test to measure social hierarchy in mice. Nat. Protoc 14, 819–831 (2019). [PubMed: 30770887]

56. Byers SL, Wiles MV, Dunn SL & Taft RA Mouse estrous cycle identification tool and images. PLoS ONE 7, e35538 (2012). [PubMed: 22514749]

57. Friard O & Gamba M BORIS: a free, versatile open-source event-logging software for video/audio coding and live observations. Methods Ecol. Evol 7, 1325–1330 (2016).

58. Fink AJP, Axel R & Schoonover CE A virtual burrow assay for head-fixed mice measures habituation, discrimination, exploration and avoidance without training. eLife 8, e45658 (2019). [PubMed: 30994457]

59. Berman GJ, Choi DM, Bialek W & Shaevitz JW Mapping the stereotyped behaviour of freely moving fruit flies. J. R. Soc. Interface 11, 20140672 (2014). [PubMed: 25142523]

60. Choi JY et al. A comparison of dopaminergic and cholinergic populations reveals unique contributions of VTA dopamine neurons to short-term memory. Cell Rep. 33, 108492 (2020). [PubMed: 33326775]

61. Pisano TJ et al. Homologous organization of cerebellar pathways to sensory, motor, and associative forebrain. Cell Rep. 36, 109721 (2021). [PubMed: 34551311]

62. Renier N et al. Mapping of brain activity by automated volume analysis of immediate early genes. Cell 165, 1789–1802 (2016). [PubMed: 27238021]

63. Chon U, Vanselow DJ, Cheng KC & Kim Y Enhanced and unified anatomical labeling for a common mouse brain atlas. Nat. Commun 10, 5067 (2019). [PubMed: 31699990]

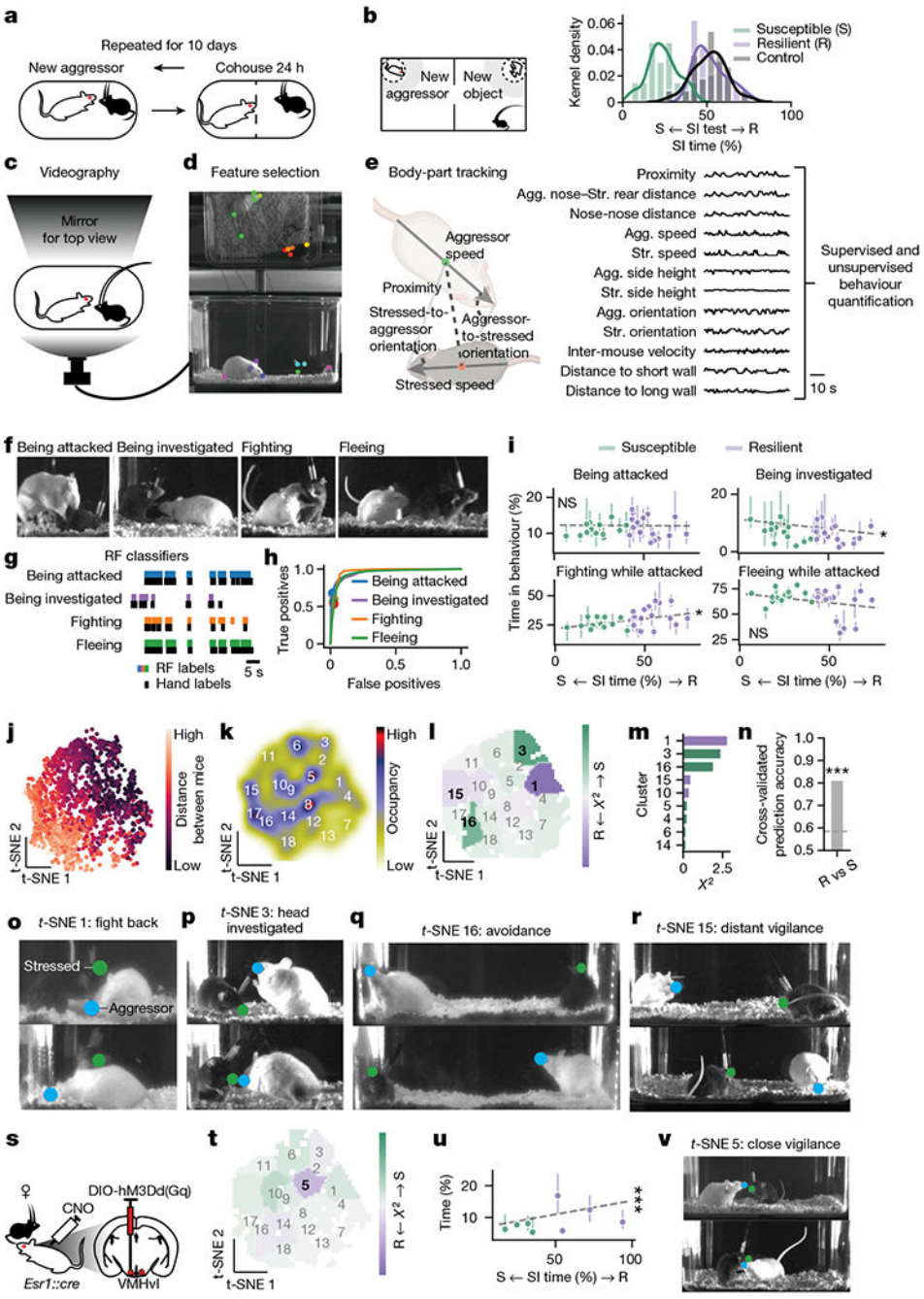

Fig. 1 |. Resilience and susceptibility can be associated with different behaviour profiles during defeat.

a, Schematic of the chronic social defeat experiment. **b**, Left, Schematic of the social interaction (SI) test. Right, The distribution of SI times in unstressed control mice (N = 22) and in resilient (N = 19) and susceptible (N = 13) stressed mice. **c**, Schematic of side and top-down views of defeat, recorded by one camera**. d**, Video frame with body-part tracking**. e**, Left, Subset of postural features (mice created with BioRender. com). Right, All 12 features for supervised (**f**–**i**) and unsupervised (**j**–**r**) behaviour quantification. **f**,

Video frames of behaviours of interest. **g**, Manual (Hand) annotation and binary random forest (RF) classification of behaviours. **h**, Behaviour classification accuracy. **i**, Relationship between time in behaviours of interest and SI time. GEEs: attacked, $P = 0.909$; investigated, $P = 0.040$; fighting, $P = 0.016$; fleeing, $P = 0.104$; $N = 32$ mice; points show means, lines show 30–70th percentile across days. **j**, *t*-SNE embedding from an example defeat session coloured by distance between mice. **k**, Smoothed histogram of *t*-SNE embeddings from all defeat sessions, with clusters numbered by increasing distance between mice. **l**, Difference in occupancy of *t*-SNE clusters between resilient ($N = 19$) and susceptible ($N = 13$) mice. Clusters with the largest differences are highlighted in bold (see **o**–**r**). **m**, Behaviours with the largest difference in **l** (purple, resilient-biased; green, susceptible-biased; same mice as in **l**). **n**, Leave-one-mouse-out cross-validation accuracy (0.81) of predicting resilience versus susceptibility from occupancy of *t*-SNE clusters; dotted line shows 1 s.d. above chance (0.5) accuracy on shuffled data (one-sided normal test for proportion > 0.5, $P = 3.0 \times 10^{-6}$; same mice as **l** and **m**). **o**–**r**, Two video frames from clusters with the largest differences between resilient and susceptible mice. **o**, *t*-SNE 1: fight back. **p**, *t*-SNE 3: head investigated. **q**, *t*-SNE 16: avoidance. **r**, *t*-SNE 15: distant vigilance. **s**, Schematic of the social defeat towards females experiment. **t**, Difference in occupancy of *t*-SNE clusters between resilient ($N = 4$) and susceptible ($N = 4$) females; the cluster with the greatest difference is highlighted in bold. **u**, Relationship between time spent in *t*-SNE 5 and SI time. GEE: $Z = 4.58$, $P = 8.6 \times 10^{-5}$, Bonferroni-corrected for 18 comparisons; $N = 8$ mice; points show means, lines show 30–70th percentile across days. **v**, Two video frames from *t*-SNE 5 (close vigilance). Across panels, $^{*}P < 0.05$, $^{**}P < 0.01$, $^{***}P < 0.001$, NS, not significant.

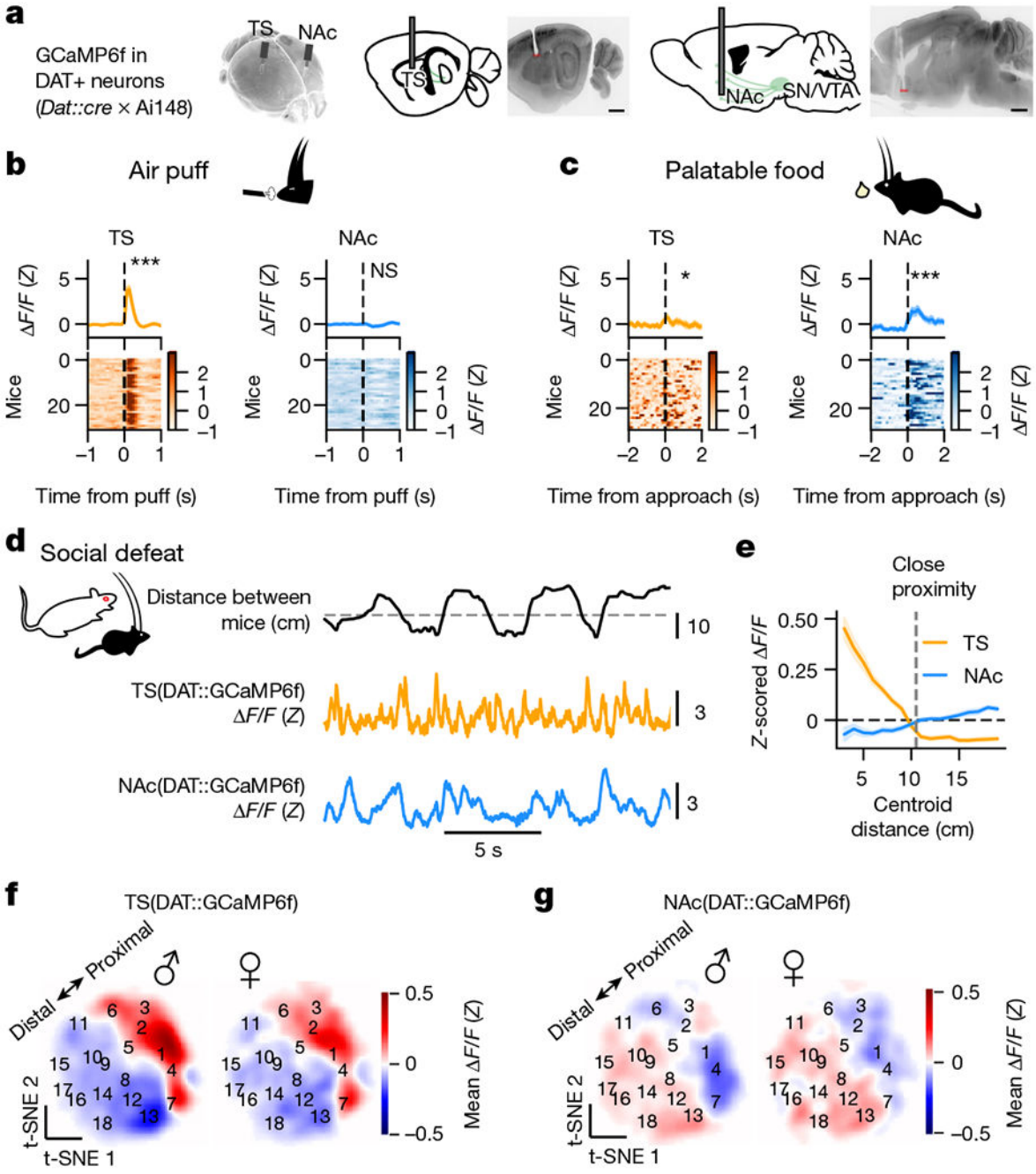

Fig. 2 |. DAT::GCaMP6f responses in the TS and NAc are oppositely modulated in proximity to the aggressor.

a, Location of fibre photometry recordings from dopaminergic (DAT$^+$) projections in the NAc and TS in the same mouse, recovered using light-sheet microscopy (representative across $N = 19$ males, 7 females). Scale bars, 400 μm (red, fibre tip diameter) or 1 mm (black) or 400 μm diameter (red, fibre tips). **b**, Average TS(DAT::GCaMP6f) (left) and NAc(DAT::GCaMP6f) (right) responses aligned to air-puff onset within and across all mice ($N = 19$ males, 8 females, paired two-sided *t*-test for average activity after versus

before puff: TS, $t = 5.11$, $P = 5.4 \times 10^{-6}$; NAc, $t = -1.34$, $P = 0.19$). **c**, Average TS(DAT::GCaMP6f) (left) and NAc(DAT::GCaMP6f) (right) responses aligned to approach onset of food reward within and across mice ($N = 19$ males, 7 females, paired two-sided t-test for average activity after versus before approach: TS, $t = 2.36$, $P = 0.025$; NAc, $t = 6.59$, $P = 3.8 \times 10^{-7}$). **d**, Example DAT::GCaMP6f traces in TS(DAT::GCaMP6f) and NAc(DAT::GCaMP6f) mice aligned to distance between aggressor and stressed mice. The grey dotted line shows the 10.5 cm threshold used to define close proximity. **e**, Relationship between distance between mouse centroids and TS(DAT::GCaMP6f) or NAc(DAT::GCaMP6f) responses. Close proximity is defined as distances below which NAc(DAT::GCaMP6f) is negative (10.5 cm). **f**, Mean TS(DAT::GCaMP6f) responses across t-SNE behaviour space in defeated males (left) and females (right). The proximal–distal line shows the axis in the behaviour map defined by proximity between mice during defeat ($N =$ 19 males, 8 females). **g**, Same as **f** but for NAc(DAT::GCaMP6f) responses. Across panels, $*P < 0.05$, $**P < 0.01$, $***p < 0.001$.

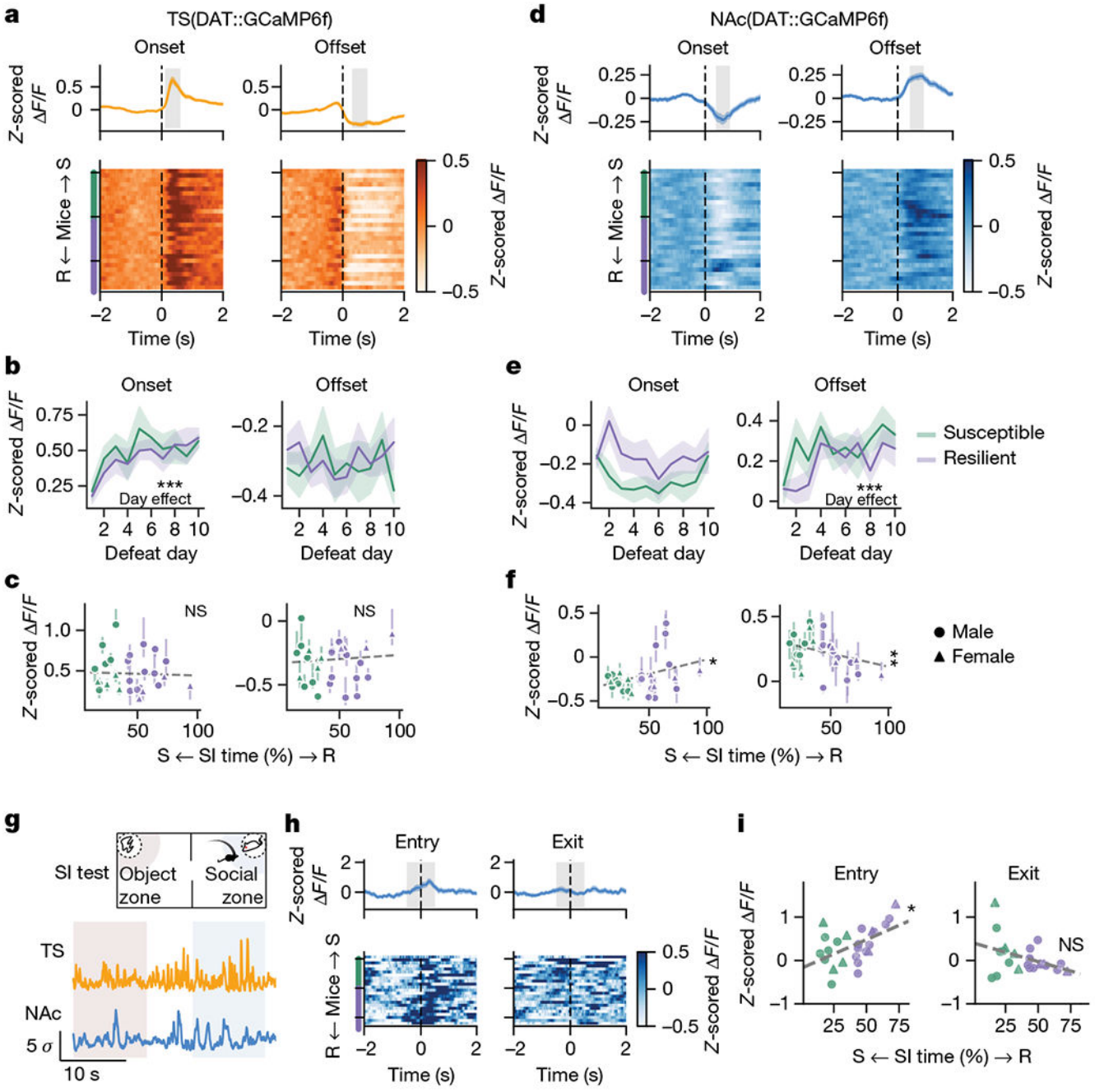

Fig. 3 |. DAT::GCaMP6f responses in proximity to aggressors in the NAc, but not the TS, are correlated with resilience.

a, Aggressor proximity onset-aligned and offset-aligned TS(DAT::GCaMP6f) responses during defeat. Data show the mean ± s.e.m. across mice and mean within mouse sorted from susceptible (green, $N = 7$ males, 4 females) to resilient (purple, $N = 12$ males, 4 females). Grey region indicates 0.5 s surrounding the extrema. **b**, Average TS(DAT::GCaMP6f) responses (grey region in **a**) from resilient and susceptible groups across defeat (mean ± s.e.m.). **c**, TS(DAT::GCaMP6f) responses (grey region in **a**) versus SI time. Two-sided GEE: onset activity by SI time, day and their interaction: main effect of SI time, $Z = -0.24$, $P =$

0.81; main effect of day, $Z = 4.973$, $P = 6.6 \times 10^{-7}$. Two-sided GEE: offset activity by SI time, day and their interaction: main effect of SI time, $Z = 0.388$, $P = 0.70$; main effect of day, $Z = -0.059$, $P = 0.953$. **d**–**f**, Same as **a**–**c**, respectively, but for NAc(DAT::GCaMP6f) responses. For **f**, GEE: onset activity by SI time, day and their interaction: main effect of SI time, $Z = 1.98$, $P = 0.032$; main effect of day, $Z = -0.93$, $P = 0.35$. Two-sided GEE: offset activity by SI time, day and their interaction: main effect of SI time, $Z = -2.77$, $P = 5.7 \times 10^{-3}$; main effect of day, $Z = 3.84$, $P = 1.2 \times 10^{-}$. **g**, Example traces of DAT::GCaMP6f in the TS and the NAc during SI test. **h**, Social zone entry-aligned and exit-aligned NAc(DAT::GCaMP6f) responses across stressed mice (mean ± s.e.m., $N = 6$ susceptible males, 4 susceptible females, 10 resilient males, 3 resilient females), **i**, Average NAc(DAT::GCaMP6f) responses in the 1 s surrounding entry or exit from the social zone versus SI time. Entry: two-sided correlation, $R = 0.51$ $P = 0.01$; exit: two-sided correlation, $R = -0.39$, $P = 0.062$; same number of mice as in **h**. Across panels, $*P < 0.05$, $**P < 0.01$, $***P < 0.001$.

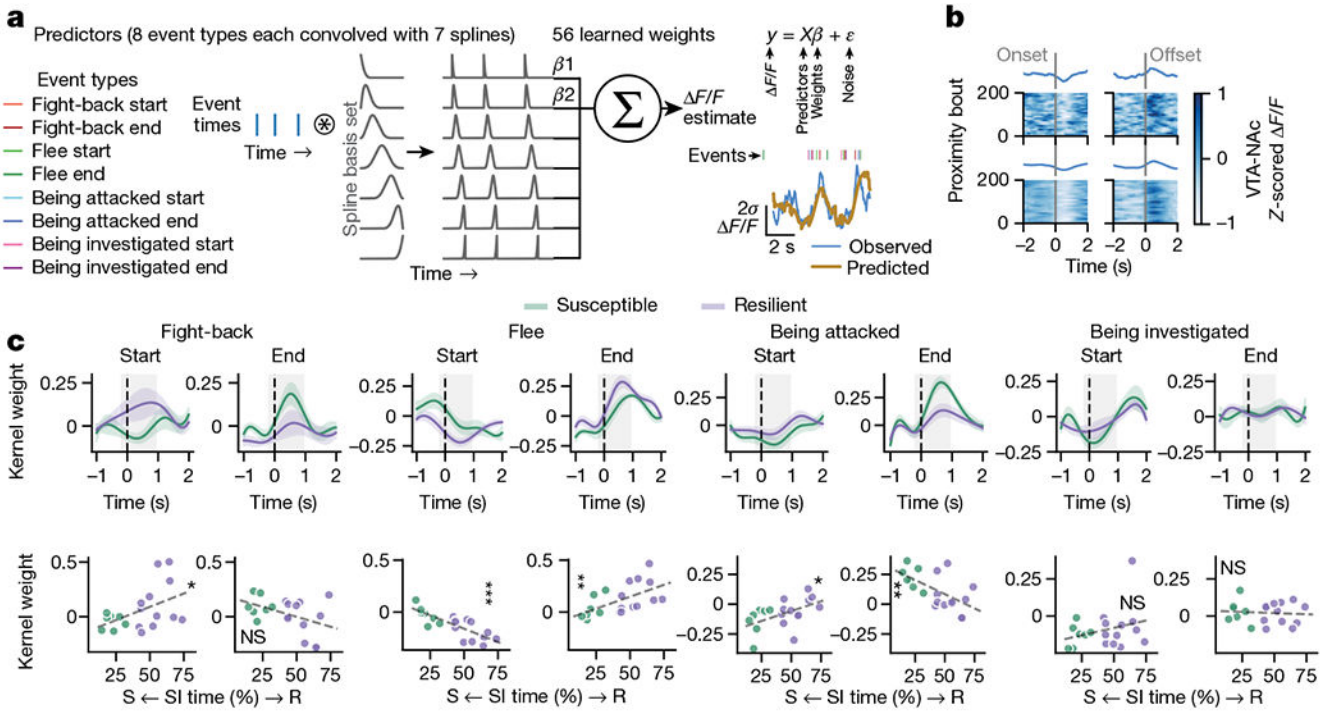

Fig. 4 |. Increased NAc(DAT::GCaMP6f) responses at the onset of fighting back are correlated with resilience, whereas increased responses at fleeing onset and attack offset are correlated with susceptibility.

a, Schematic of the linear encoding model for the relationship between behavioural events and NAc(DAT::GCaMP6f) responses. Far left, The full list of behavioural event types. Centre, The convolution of events of one type with 7 cubic splines spanning from 1 s before to 2 s after the event to produce the predictors for the model associated with that event. Right, The learned weights (β values) multiplied by the corresponding predictors sum to estimate the neural activity. An example of behaviour events and observed and predicted NAc(DAT::GCaMP6f) responses. **b**, Example of observed (top) and model-predicted (bottom) NAc(DAT::GCaMP6f) responses across all the social proximity bouts across defeat from an example mouse, aligned to onset (left) and offset (right) of proximity. **c**, Kernels for behavioural events, averaged across individuals in resilient and susceptible groups (top; mean ± s.e.m. plotted). Relationship between individual's SI time and average kernel weight in the shaded region in the above kernel weight plots (bottom). Two-sided Pearson's correlation between SI time and average kernel weight: fight onset, $R = 0.47$, $P = 0.043$; fight offset, $R = -0.43$, $R = 0.065$; flee onset, $R = -0.80$, $P = 3.7 \times 10^{-5}$; flee offset, $R = 0.58$, $P = 0.009$; attacked onset, $R = 0.51$, $P = 0.025$; attacked offset, $R = -0.60$, $P = 0.006$; investigated onset, $R = 0.28$, $P = 0.24$; investigated offset, $R = -0.08$, $P = 0.74$. In all panels, $N = 7$ susceptible, 12 resilient males. $^{*}P < 0.05$,$^{**}P < 0.01$,$^{***}P < 0.001$.

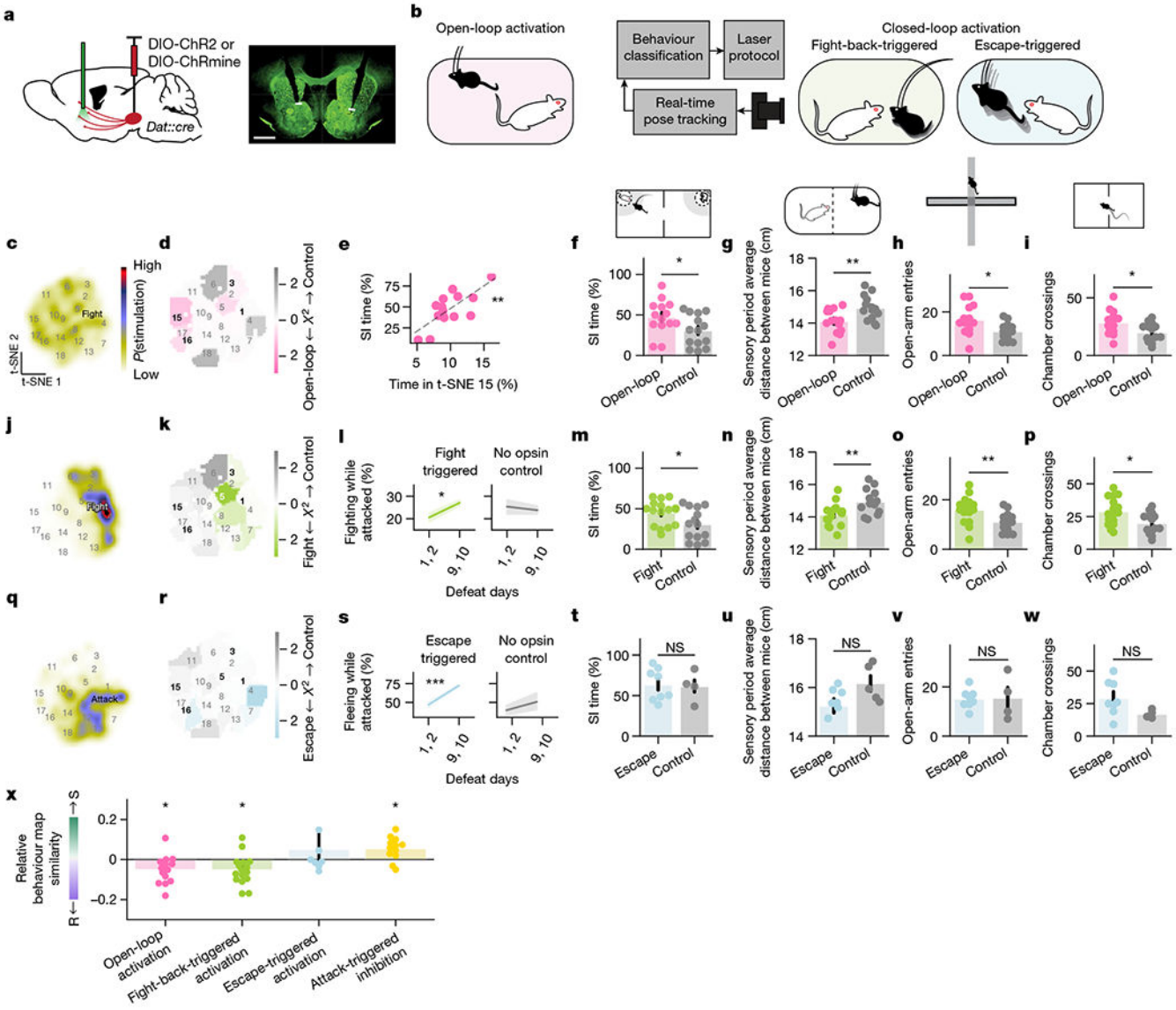

Fig. 5 |. DAT::NAc activation during defeat can bias individuals towards resilience.

a, Left, Neural activation strategy. Right, example histological image with fibre placement. Scale bars, 200 μm (fibre tips) or 1 mm. **b**, Schematic of open-loop and closed-loop optogenetics. **c**, Probability of stimulation across behaviour space in the open-loop activation group. **d**, *t*-SNE cluster occupancy difference between open-loop ($N = 14$ males) and control ($N = 14$ males) groups (same mice for **e**–**i**). Highlighted in bold are groups differentially expressed by resilient and susceptible mice in our observational study (Fig. 1). **e**, Across open-loop activation mice, SI time versus average time in *t*-SNE 15 (distant vigilance; see also Fig. 1r). Two-sided correlation $R = 0.74$, $P = 0.0026$, $N = 14$. **f**, Difference in SI time between open-loop and control groups ($t = 2.19$, $P = 0.037$). **g**, Difference between open-loop and control groups in average distance between stressed and aggressor mice during the first 5 min of the barrier-separated sensory period ($t = -2.90$, $P = 0.008$). **h**, Difference in open-arm entries in the elevated plus maze between open-loop and control groups ($t = 2.56$,

$P = 0.016$). **i**, Difference in chamber crossings in the two-chamber arena between open-loop and control groups ($t = 2.45$, $P = 0.02$). **j**,**k**, Same as for **c** and **d**, respectively, but for fight-back-triggered activation ($N = 16$ males) and control ($N = 14$ males) groups (same mice for **l**–**p**). **l**, Time spent in fighting behaviour early (day 1 and 2) versus late (day 9 and 10) in defeat. Paired *t*-tests: two-way false discovery rate (FDR) corrected: fight-back-triggered, $t = 2.77$ $P = 0.029$; control, $t = -0.41$ $P = 0.69$. **m**, Same as **f**, but for fight-back-triggered activation ($t = 2.29$, $P = 0.030$). **n**, Same as **g**, but for fight-back-triggered activation ($t = -2.99$, $P = 0.006$). **o**, Same as **h**, but for fight-back-triggered activation ($t = 2.87$, $P = 0.008$). **p**, Same as **i**, but for fight-back-triggered activation ($t = 2.64$, $P = 0.013$). **q**,**r**, Same as **c** and **d**, respectively, but for escape-triggered activation ($N = 8$ males) and control ($N = 5$ males) groups (same mice for **s**,**u**,**v**). **s**, Time spent fleeing early (day 1 and 2) versus late (day 9 and 10) in defeat. Paired *t*-tests: two-way FDR corrected: escape-triggered, $t = 6.42$ $P = 7.2 \times 10^{-4}$; control $t = 0.68$, $P = 0.54$. **t**, Same as **f**, but for escape-triggered activation ($t = 0.17$, $P = 0.87$, $N = 8$ experimental, 4 control mice). **u**, Same as **g**, but for escape-triggered activation ($t = -3.94$, $P = 0.07$). **v**, Same as **h**, but for escape-triggered activation ($t = -0.10$, $P = 0.92$). **w**, Same as **i**, but for escape-triggered activation ($t = 1.76$, $P = 0.11$, $N = 8$ experimental, 4 mice). **x**, Relative similarity in *t*-SNE behaviour maps from individuals in manipulation groups to susceptible or resilient males in our observational study (see also Fig. 1). One-sample, two-sided *t*-tests for mean different from 0, four-way Benjamini–Hochberg FDR corrected: open-loop, $t = -2.73$, $P = 0.023$; fight-back-triggered, $t = -2.85$, $P = 0.023$; escape-triggered, $t = 1.11$, $P = 0.30$; attack-triggered inhibition, $t = 3.3$, $P = 0.023$. In panels **f**–**i**, **m**–**p**, **t**–**w**, two-sided *t*-test was used. Across panels, the bar and line plots show the mean ± s.e.m., $*P < 0.05$, $**P < 0.01$, $***P < 0.001$.